CHALMERS
UNIVERSITY OF TECHNOLOGY

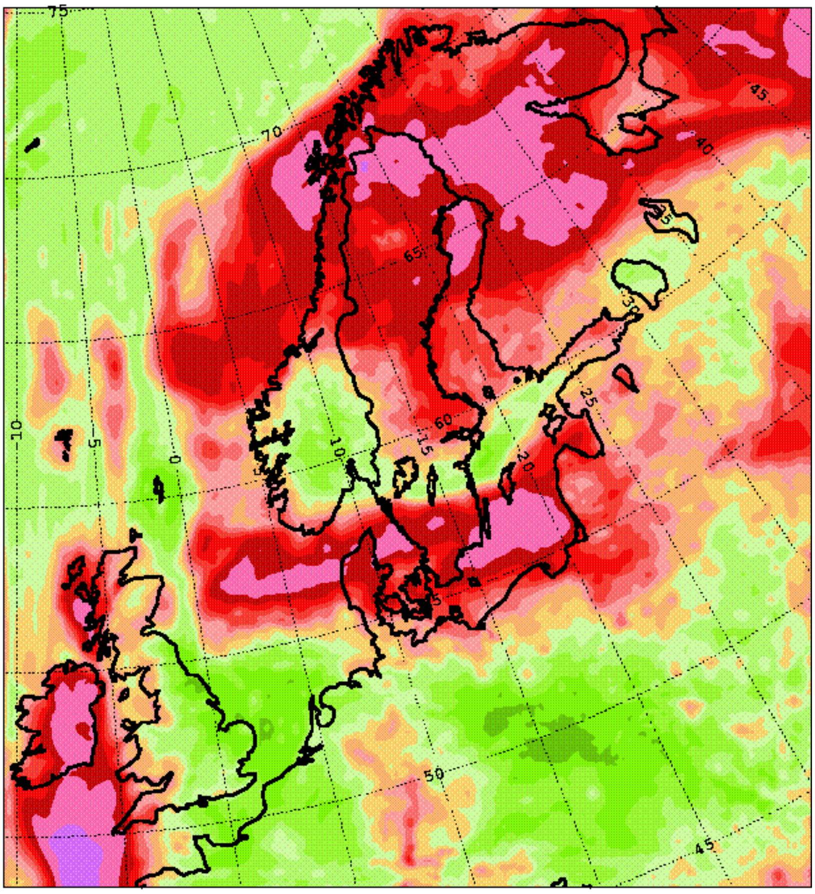

Control and design of Quasi-Z-Source Inverter (qZSI) for grid connected Photovoltaic (PV) arrays

Master's thesis in Electric power engineering

SHREY SHARMA

Department of Electrical Engineering
CHALMERS UNIVERSITY OF TECHNOLOGY
Gothenburg, Sweden 2018

Master's thesis 2018:NN

Control and design of Quasi-Z-Source Inverter (qZSI) for grid connected Photovoltaic (PV) arrays

SHREY SHARMA

CHALMERS
UNIVERSITY OF TECHNOLOGY

Department of Electrical Engineering
Division of Electric power engineering
Chalmers University of Technology
Gothenburg, Sweden 2018

Control and design of Quasi-Z-Source Inverter (qZSI) for grid connected Photovoltaic (PV) arrays

SHREY SHARMA

Supervisor & Examiner: Prof. YUJING LIU, Department of Electrical Engineering

Master's Thesis 2018:NN
Department of Electrical Engineering
Division of Electric power engineering
Chalmers University of Technology
SE-412 96 Gothenburg
Telephone +46 31 772 1000

Cover: Global irradiation (Wh/m^2) on the 30th of May, 2013 obtained from Swedish Meteorological and Hydrological Institute (SMHI).

Typeset in LaTeX
Gothenburg, Sweden 2018

Abstract

The renewable energy sources are greener and more environment friendly than non-renewable energy sources. They are used for the sustainable power production. Solar energy is abundant in a lot of places and can be tapped to satisfy energy needs. The Photovoltaic(PV) arrays can be connected to an inverter to convert DC output of PV cells to AC supply for the grid. A type of converter that we can use for this application is Quasi-Z-Source Inverter(qZSI). In this project, one of the task has been to calculate and verify the value of elements used in the qZSI. The verification was done by pole-zero maps, bode plots and through optimization via simulations of the model.
This was followed by designing a controller for the DC side of the qZSI. Since it was for DC side, it is called the DC side controller. Its design involved verification of the transfer functions derived from the signal flow graph using Mason's gain formula. The signal flow graph comes from the dynamic model of the qZSI. The block diagram from the transfer function was then simplified so as to apply the Internal model control(IMC) principle to obtain the proportional and integral constants(for the inner and outer loop) of the controller. The inner loop is for the inductor current while the outer loop is for the DC link voltage. These were later fine-tuned to another set of proportional and integral controller constants when both loops were cascaded.

Later, comparison of the output of qZSI's Simulink model was done with the Fronius IG 15 inverter installed in Chalmers Grundkurs lab. It was also compared with a reference model*(already available in Simulink library which was optimized for comparison with qZSI) which is Simulink model of a VSI connected with a boost converter supplying the grid. The input for it is DC supply from PV arrays. For comparison it was important that the DC input remained same for both the models; the MPPT voltage input to VSI was sampled and used as input for qZSI model. The fast fourier transform(FFT) and total harmonic distortion(THD) measurement of the output of all three inverters was compared. It was found that the Fronius inverter had the least THD followed by VSI and then the qZSI. In all cases, THD was well within the limit as per IEEE standard STD 519-2014. The FFT showed presence of lower odd harmonics in all three inverters. The magnitude of odd harmonics upon FFT followed the same suit as the THD.
All in all, a much more fine tuned controller and better filters can be designed for the qZSI to decrease the harmonics content. A better switching strategy can also be used to eliminate the harmonics. Considering that qZSI has a single stage unlike the reference model* with cascaded boost and VSI inverter, it is cost effective to use qZSI plus it can perform both the buck and boost operations. This makes it an attractive replacement option of VSI for usage in applications like PV array and fuel cells.

Keywords: Photovoltaic(PV), Voltage source inverter(VSI), Harmonics, Impedance/Z-source inverter(ZSI), Quasi-impedance/Z-source inverter(qZSI), Shoot-through, Total Harmonic Distortion(THD), Pulse width modulation(PWM), Internal model control(IMC), Boost factor.

Acknowledgements

First of all, I would like to express my gratitude towards my examiner and supervisor Prof. Yujing Liu for being incredibly patient and supportive at all times and for various technical inputs, ideas and encouragement I got from him.

I would also like to thank Prof Ola Carlson, Magnus Ellsen and Nima Saadat for the discussions and help in data collection. I also appreciate Swedish Meteorological and Hydrological Institute (SMHI) and Curtis J Blank for their help in sourcing more data.

Thanks to Junfei Tang, Ankit Gupta and Ehsan Behrouzian for all their help, availability and technical discussions. I also appreciate and thank my fellow master's students Nimananda Sharma, Shivadeep Maheshwar and Somadutta Sahoo for support, suggestions and discussions. They made the thesis work a great experience.

Finally, I would like to express profound gratitude towards my family for their constant support and advice.

SHREY SHARMA, Gothenburg, Jan. 2018

Contents

List of Figures

List of Tables

1
Introduction

Fuelled by the energy derived by fossil fuels the growth engine of the world had been moving pretty fast in the past century but with time people realized the effect of pollution, coal mining and oil drilling on the environment. Currently sustainable growth can be realized with clean energy initiatives.With the rise in the quality of life in countries around the world, the energy consumption is also increasing. This means more loading on non-renewable energy sources. The solution of problem lies in turning to clean energy sources like solar, water, wind energy, etc.

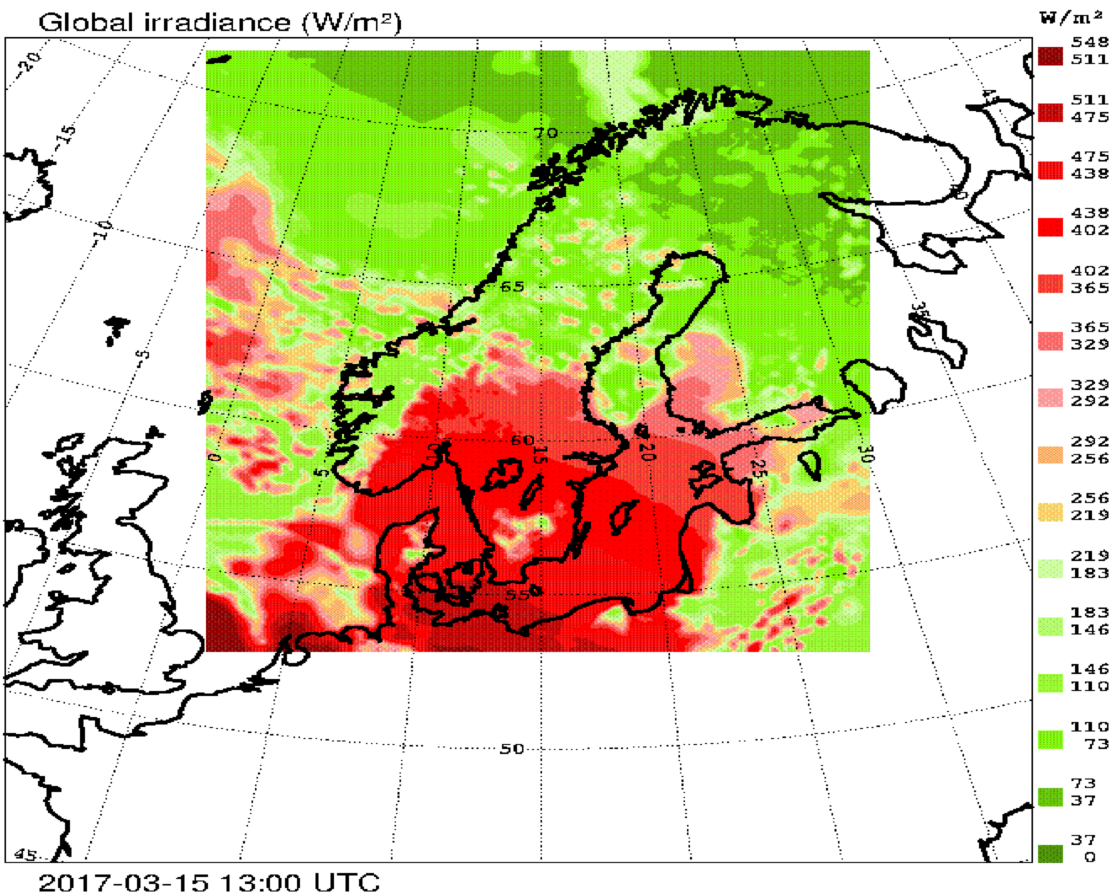

Figure 1.1: Global irradiation (Wh/m^2) on the 15th of March, 2017 obtained from Swedish Meteorological and Hydrological Institute (SMHI)[1]

The potential of solar energy is quite high not only in Sweden [2] but also in sun rich places like China, India where the goal is to increase installed capacity to 100 GW by both the countries [3]. Other countries also have achievable goals for installed capacity in solar energy segment [4].
The decrease in cost and conducive government policies are a good impetus vitalizing the growth of solar energy sector. In recent years, tremendous increase in the installed capacity has been observed worldwide, especially concentrated in China, Japan and the USA followed by India, Germany, South Korea, Australia, France and Canada. Although the leaders for solar Photovoltaic(PV) energy generation per person are Germany, Italy, Belgium, Japan and Greece yet China leads in terms of cumulative installed capacity with its share exceeding more than 19% of the net world capacity.[4]

In current times, distributed power generation is becoming more accepted [5]. In case of distributed power generation, the sources are spread over a range of geography and are mostly renewable energy sources thus environment friendly.The drawback in distributed generation though is production of power at different voltage and frequency for different sources. Such is a common phenomenon in sources like fuel and photovoltaic cells. Since such variation occurs during power production it is necessary to standardize the inverter operation [6] whether it is grid tied or isolated. Since the voltage varies, an inverter with boost converter or another type of inverter called Quasi-Impedance source inverter(qZSI) is used.

1.1 Aim

The main aim of the thesis is to design a Quasi-Impedance source inverter(qZSI) of power rating 10 kW and switching frequency 10 kHz, its DC side controller and compare the power quality(PQ) of the output with an already available Simulink library model of a grid connected Voltage source inverter(VSI) referred as reference model* hence forth here. Both the models are for Photovoltaic (PV) arrays connected to the grid. The output PQ of designed qZSI is also compared with that of an installed Fronius solar inverter in the Chalmers Grundkurs lab.

1.2 Sustainable development and ethical aspects

The sustainable and ethical aspects of the qZSI design and PQ comparisons can be looked in a larger perspective of sustainable development and usage of solar power. When we see this picture certain points do come up.
Since power production through renewable energy sources is a primary need for sustainable development, solar power production with better PQ is a step in that direction. Tapped solar energy fed into the grid effectively reduces the burden on non-renewable energy sources for power production. Over the period 2017-2022 the International Energy Agency (IEA) forecasts that the renewable energy segment around the world shall grow by over net 920 GW with an increment of 43% compared to the period 2011-2016 and the biggest portion of it shall be the solar energy

[7]. This leads to one of the issues that readily available resources for a cheap price tend to be wasted as well. The more cheap power is produced, chances are that it is utilized less wisely. Another aspect to consider is what would be the effect of increased demand for PV arrays for producing solar power. There are gases like nitrogen trifluoride and sulfur hexafluoride produced during the solar PV cell manufacture which contribute to global warming more than the carbon dioxide. Also usage of materials like cadmium telluride (CdTe) or copper indium gallium selenide (CIGS) for thin film solar cells is a point to consider and figure out the after effects on the environment and the manufacturing populace [8].
Hence the question raised in relation to impact of PQ comparison for qZSI with other inverters to sustainable development is: *what will be the impact in terms of sustainable development if PQ is better for qZSI?*

There are some project specific risks which have been identified over here. The first project specific risk is to *involves providing the correct results obtained from measurements and simulations in order to make fair comparisons among the three inverters.* Another risk that comes to notice is: *necessity of being critical of the data and information provided by manufacturer for the sake of fairness of comparison.* In case manufacturer has a business stake in consulting, chances of benefits from planting business conducive information have to be taken in account as well.

1.3 Scope

The PQ comparison is only with respect to the harmonic content and other PQ aspects are not considered. Only the DC side controller was designed again due to time constraints.
The comparison has been done for a moderate time length of 1.2 sec in case of simulated models while only an instant data is considered for Grundkurs lab Fronius inverter. The difference in switching frequency between the models and the Fronius inverter is not considered. The Total Harmoinc Distortion (THD) plots are added for the models since they span for the simulated time while THD value for Fronius inverter is stated. In case of sampling of reference model* MPPT voltage for usage as input in qZSI model, low sampling frequency of 10 kHz is used for quicker sampling compared to the sampling frequency used in Fronius inverter's data sampling.

1.4 Thesis structure

The thesis is divided into the following parts:
- Introduction to PV arrays and Fronius inverter installed at Chalmers and Grundkurs Lab respectively,
- Insight of the inverters and theory, operation of ZSI/qZSI,
- Method to design the qZSI and its DC side controller,
- Comparison results, discussion and conclusion.

2

Photovoltaic array and inverters

2.1 Photovoltaic(PV) array

Photovoltaic(PV) cells form the basic unit of PV generators. The PV cells can be connected in to form bigger units of PV power production called PV modules. A lot of PV modules can be connected either in series and/or in parallel to form PV arrays. The PV arrays can be connected electrically to form PV generators. The amount of power produced by the basic unit i.e. PV cell varies from 1 to 2 W [10]. But with formation of larger electrical units like PV arrays, they produce power in the range of MW as well.
The single-diode circuit is one of the simplest yet fairly accurate model of PV cells. There are other equivalent circuit models like the two-diode circuit model or the three-diode circuit model which account for factors like effect of charge carrier recombination and large leakage current on the PV cell respectively. The Figure 2.1 represents single-diode equivalent circuit model of a PV cell, where I_g is the current source in parallel with a diode and parallel resistance R_p. The diode current is I_d, I_i is the terminal current of the ideal PV cell while the series resistance is R_s. In equation 2.1, I and V are the PV cell terminal current and voltage respectively .

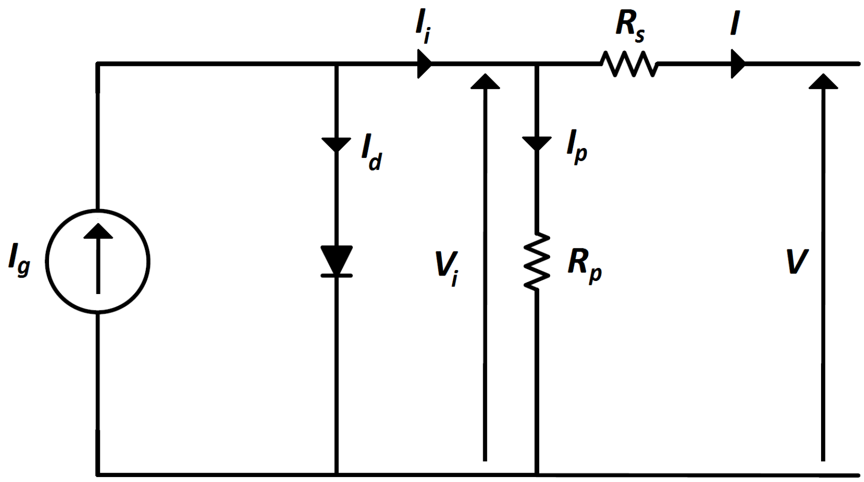

Figure 2.1: Single-diode equivalent circuit of a PV cell.

The equation 2.2 describes the non-linear current-voltage relationship of the PV cell where a is the diode ideality factor, β is the inverse thermal voltage and I_o is diode reverse saturation current.

$$I(V) = I_i(V) - I_p(V), \quad = I_g - I_d(V) - I_p(V) \tag{2.1}$$

$$I(V) = I_g - I_o(e^{\frac{\beta(V+R_s I)}{a}} - 1) - (\frac{V + R_s I}{R_p}) \tag{2.2}$$

The inverse thermal voltage β can be obtained by equation 2.3 where k is Boltzmann's constant, q is the electron charge and T is p-n junction temperature.

$$\beta = \frac{q}{kT} \tag{2.3}$$

Figure 2.2: The PV arrays at the southern side of Electric power engineering building, Chalmers University, Johanneberg campus. Picture Credits[11]

The above image in Figure 2.2 shows the PV panels installed at the southern side of the building of Electric Power Engineering building at Johanneberg campus of Chalmers university. The solar panels are 18 in number and of model GPV110M(Gällivare Photovoltaic AB). The panels consist of 72 monocrystalline cells each with one maximum power output of 110W (Peak power). Thus, the 18 panels should ideally be able to deliver 1.98 kW together. The image in Figure 2.3 is of Fronius IG15 solar inverter, manufactured by Fronius international GmbH and installed at Chalmers Grundkurs lab.

Important details of the solar inverter in Grundkurs lab[11].

- The inverter model is Fronius IG 15 and it was installed in May 2007,
- The inverter has max power of 2 kW and voltage range of 150-400 V,
- It has a HF transformer to boost the voltage and the advantages of using the transformer are:
  - size of inverter becomes very small,
  - the inverter becomes light and powerful,
  - The transformer provides safety due to electrical isolation.

Figure 2.3: Fronius IG 15 inverter installed in Chalmers Grundkurs lab, Johanneberg campus.

The Figure 2.4 is block representation of grid connection of the PV panels and solar inverter installed at Chalmers Johanneberg campus.

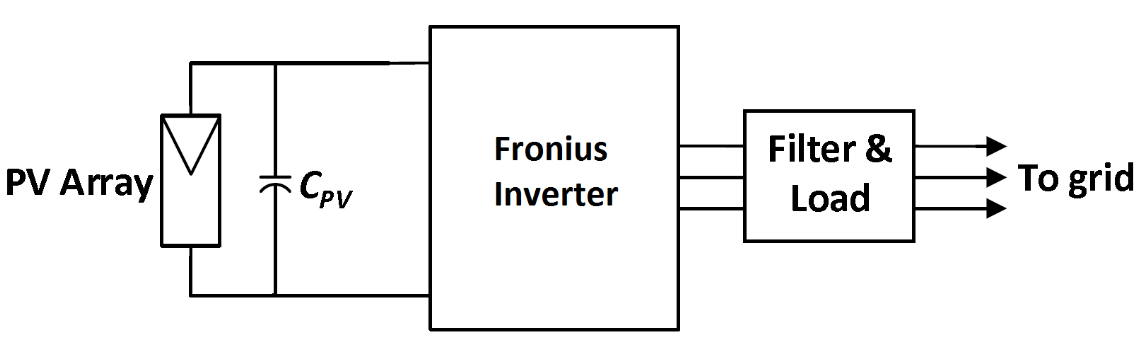

Figure 2.4: Simplified representation of grid connected PV array system at Chalmers.

2.2 Converters

Of the multiple types of converters, an inverter converts DC-AC with variation in magnitude and frequency while the AC-DC conversion takes place by a rectifier with adjustment in voltage and current. Other than the mentioned converter types, AC-AC and DC-DC converters are also present. The DC-DC converters are one of the most widely used converters.

2.2.1 DC-DC converters

A simple model of DC-DC boost converter is shown in Figure 2.5.

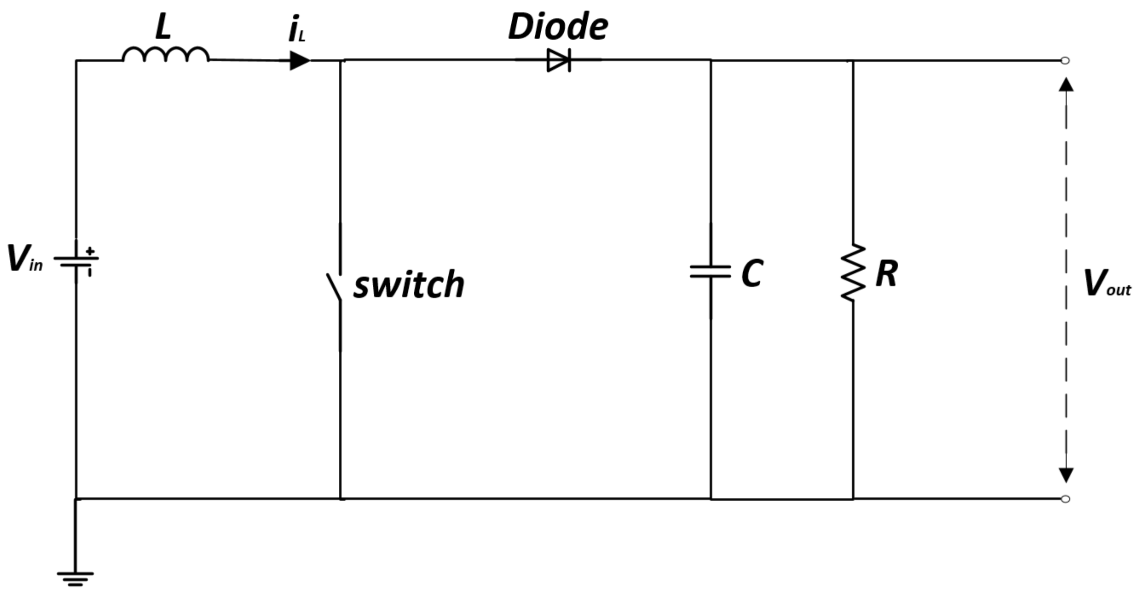

Figure 2.5: Simple DC-DC boost converter circuit.

The major types of DC-DC converters are: Buck, boost, buck-boost and flyback converters. There can be classified as isolated and non-isolated types of converters.

The flyback converter belongs to the category of isolated converters while the buck, boost and buck-boost converters belong to the non-isolated converter category. The isolated converter have a galvanic isolation wherein a transformer is used unlike the non-isolated converters with no electrical isolation.
Apart from the mentioned popular converters, there are other converters as well like the Ćuk converter and the charge pump. The Ćuk converter is a non-isolated type of converter. The function of various DC-DC converters is to vary the supplied output voltage. The boost converter is a voltage step-up converter and buck on the other hand is a voltage step-down converter. Since the power remains constant the current falls in boost while rises in buck converter. The buck-boost can do both the step-up and step-down of output voltage. The flyback and Ćuk have the same function as buck-boost converter. The flyback converter has an isolating factor due to the presence of transformer separating input from output. The usage varies from cell phone chargers and LASERS to standby power supplies in PCs. The charge pump converter on the other hand is basically used for low power applications. It is also similar in function to the buck-boost converter.

2.2.2 Inverters

The inverters can be classified into two broad types: voltage source inverter(VSI) and current source inverter(CSI). The VSI is a voltage step down/buck inverter while the CSI is a voltage boost/step up inverter.
The traditional voltage source inverter (VSI) system is as shown in Figure 2.6

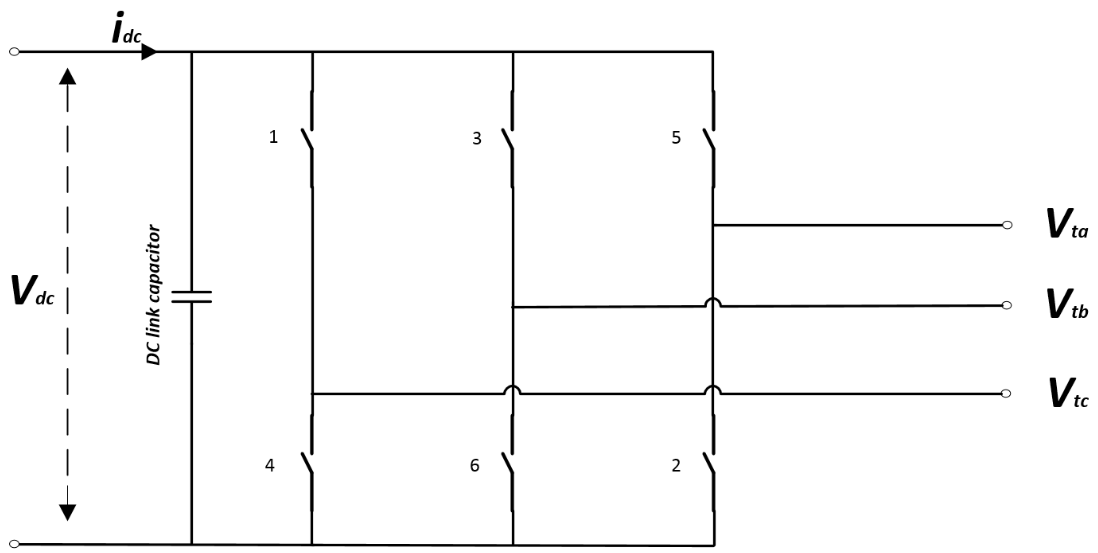

Figure 2.6: Schematic diagram of a Voltage Source Inverter system.

The VSI has a voltage source connected in parallel with a large capacitor while CSI has a current source as input. The CSI directly controls output AC current. Thus, the VSI is a voltage stiff inverter while the CSI is a current stiff inverter. The usage

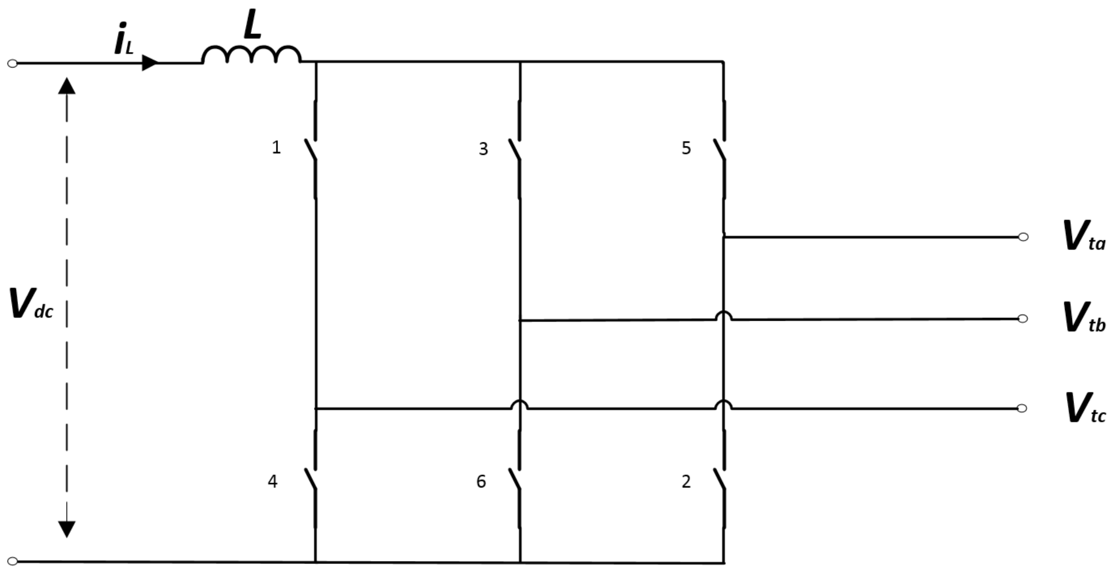

Figure 2.7: Schematic diagram of a Current Source Inverter system.

of VSI is in uninterruptible power supply(UPS) units, adjustable speed drives(ASD) for ac motors, electronic frequency changer circuits, etc.
A traditional current source inverter (CSI) system looks like as shown in Figure 2.7. Of the two types, VSI is more used than the CSI in industry. In this work also we shall deal with VSI and later with Quasi-impedance source inverter(qZSI).

2.2.3 The drawbacks and limitations of VSI and CSI

Of the two types of inverters, the VSI though used more often has certain drawbacks and limitations mentioned below:

- The VSI is a voltage buck converter and consequently can't be used in places where input voltage is low compared to the output voltage(required operation is buck). In the case of fuel cells and photovoltaic applications, a boost converter is used in conjunction with the VSI to obtain a voltage step-up. Since another converter is also used, it leads to increased cost and decreased efficiency.
- Simultaneous operation of the two legs of a phase is not possible since it will lead to the source shorting, a situation called shoot-through and hence the destruction of the switches. Therefore a blanking time is introduced which again leads to increased harmonics.
- Compared to CSI a bigger LC filter is needed at the VSI output in order to provide a near sinusoidal voltage, leading to loss of power and decreased efficiency.

The I-source inverter(CSI) also has some limitations and ceilings mentioned below:

- The CSI is a voltage boost converter. So in certain cases a buck/boost converter is used prior to the CSI to step-down/up the input voltage to the CSI. Since another converter is also used, it leads to increased cost and decreased

efficiency(because there is another power conversion stage due to extra converter).
- High preformance of the IGBT's is decreased owing to the usage of a series diode in combination.

In addition, both VSI and CSI share the following problems:
- Since they are either a voltage buck or voltage boost inverter and not buck-boost, their application is limited for certain scenarios because of range of output voltage achievable.
- The VSI and the CSI cannot be interchanged i.e. one used in other's place because of the different source needed and output voltage range.
- They are both susceptible to electromagnetic interference(EMI) noise.

2.3 Z-Source Inverter(ZSI)

The VSI and CSI have limitations of operation since they can act either as voltage buck or voltage boost inverter respectively, although extensively utilized in the industry [12]. Thus a boost converter is attached prior to the VSI in case of fuel cells or photovoltaic applications and similarly another DC-DC converter needs to be attached prior to a CSI to generate necessary output voltage. Since it is a tedious process to control two converters(DC-DC converter and the inverter) along with escalation in the costs, Z-source inverters(ZSI) are preferable to them. The ZSI is a single stage inverter with criss-cross of capacitor and inductor to form a X structure between the DC source and the inverter. This helps in operating both in the buck and boost mode depending upon requirement. The special network of two inductor and two capacitors uses shoot through state to achieve buck and boost in the same configuration as per the need. In case of a shoot-through state, the switches in the phase leg are simultaneously shorted. It could be one phase leg at a time, two phase legs or even all of the three.

The configuration of a ZSI is shown in Figure 2.8.

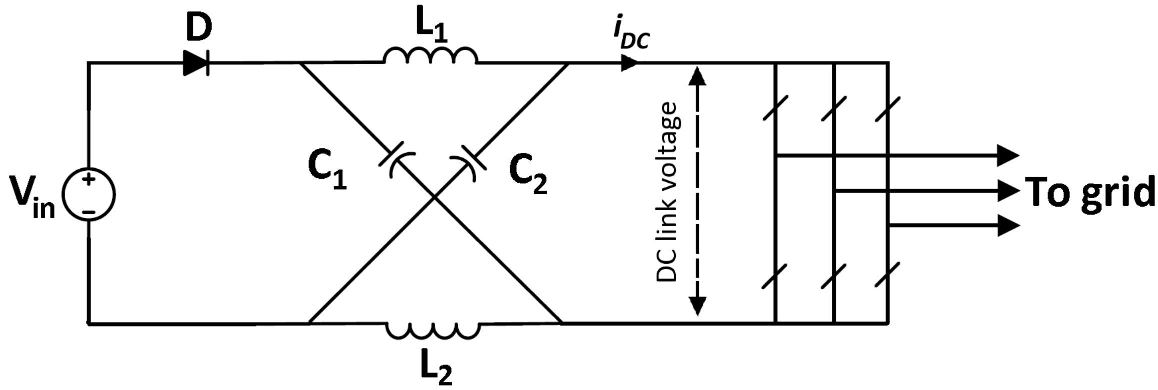

Figure 2.8: Schematic diagram of a Z-Source Inverter system.

The Figure 2.8 shows the general Z-source inverter structure consisting of two inductors $L1$ and $L2$ while capacitors $C1$ and $C2$ connected in a criss-cross X shape to couple the inverter to the DC voltage source.

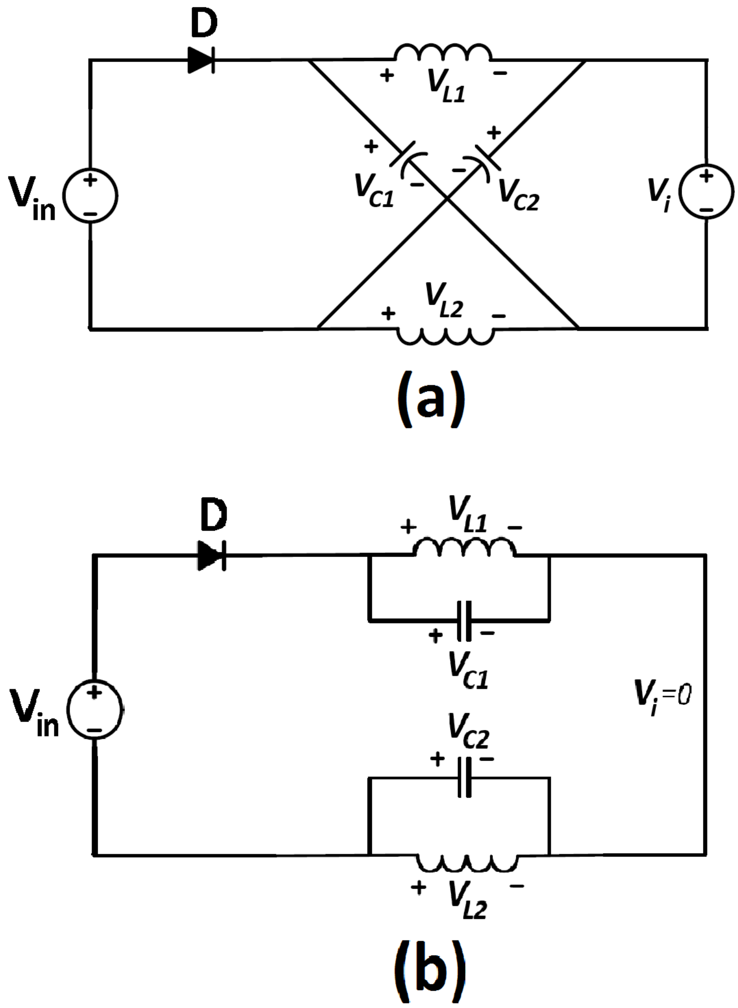

Figure 2.9: (a) Non shoot-through state equivalent circuit model of ZSI. (b) Shoot-through state equivalent circuit model of ZSI.

In case of usage of photovoltaic cells and fuels cells as DC voltage source, a boost converter is needed since the output voltage of the cells is highly variable depending on the irradiation and current drawn from the fuel stack respectively. The boost converter ensures a step-up of voltage since the VSI is avoltage buck converter. On the other hand, ZSI is a single stage inverter capable of producing both the buck and boost of AC output depending on the requirement. The VSI has six active states and two zero states but in the case of ZSI there is an additional zero state known as the shoot-through state. Thus, in all a ZSI has nine states. The shoot-through state helps in achieving a voltage boost if needed. It also ensures no need of blanking time which is a standard feature of VSIs to avoid source short circuit.
The ZSI thus has two operation modes: the regular non shoot-through mode and the shoot-through mode. The Figure 2.9 shows the equivalent circuits of ZSI at the

regular i.e. non shoot-through mode and the extra mode i.e. shoot-through mode. In the non shoot-through mode shown in Figure 2.9(a), the ZSI operates like a VSI or a CSI with the regular eight states(six active and the remaining two zero states) while in the shoot-through mode shown in 2.9(b), the source is shorted across one or all phase legs forbidden in a traditional inverter.

2.4 Advantages and disadvantages of ZSI

The ZSI in Figure 2.8 interfaces the DC source voltage and the inverter bridge. The ZSI not only has a buck-boost feature but also lacks the traditionally present blanking time in a regular inverter. The advantages ZSI poses over the traditional VSI or CSI is not limited but extends to the following:

- The DC source of input is not limited to a battery but can be one of the multitude including voltage or current source or even load like diode rectifier, thyristor converter, inductor, capacitor, etc ;
- The ZSI can be used in a plethora of applications like in variable output voltage sources such as fuel cells and photovoltaic arrays. The AC voltage can thus be varied to any value in the range of zero to very high magnitudes. The ZSI is a buck-boost inverter which is not a property of VSI or CSI;
- One can use all PWM schemes to control the ZSI. Hence, it offers great flexibility as well;
- It can be applied to all ranges of power conversion.

Current source inverter	**Voltage source inverter**	**Z-source inverter**
1.The CSI acts as a constant current source or current stiff since a large inductor is used in series with the voltage source	The VSI acts as a constant voltage source or voltage stiff inverter since a large capacitor is used in parallel with the voltage source.	The ZSI acts as a constant high impedance voltage source.
2.High source impedance due to large inductor connected in series with the DC source.	Low source impedance due to a capacitor connected in parallel with the DC source.	Since both inductor and capacitor are used in the DC link, it has a constant high impedance.
3.The CSI is more robuist and has the capacity to bear misfiring of the switches without danger, hence less sensitive comparative to the VSI.	Misfiring of switches in a VSI is dangerous since the parallel capacitor shall the fault and hence more sensitive to switch misfirings than CSI.	The ZSI can also bear misfiring of the switches sometimes though not as much as the CSI but more than the VSI.
4.Cannot be used in both buck or boost operation of inverter at the same time.	Cannot be used in both buck or boost operation of inverter at the same time.	Can be used in both buck and boost operation of inverter at the same time.
5.The main circuits are not interchangeable.	The main circuits are not interchangeable.	Here the main circuits are interchangeable.
6.The harmonic distortion tends to be high.	VSI also has quite high harmonic distortion.	Harmonic distortion in ZSI tends to be lower.
7.Introduction of filter causes high power loss.	Introduction of filter causes high power loss.	Compared to the VSI and CSI, lower power loss.
8.Observed that power loss decreases efficiency here.	High power loss decreases efficiency here.	Comparatively higher efficiency due to lower power loss.

Table 2.1: The comparison of ZSI to CSI and VSI.

2.5 Quasi-Z-Source Inverter(qZSI)

The Quasi-Z-source/quasi impedance source inverter(qZSI) is an upgrade of impedance source inverter(ZSI). It offers various advantages compared to the ZSI itself and hence has been used in the Simulink model and compared with the reference model* later. Upon doing the circuit analysis of the qZSI, we realize that almost all the equations for ZSI hold true for qZSI as well.
The main differences between the ZSI and qZSI are:
(1) The current drawn by qZSI is constant DC current while the ZSI draws discontinuous current from the source leading to less harmonics.
(2) the applied voltage and consequently the size of capacitor $C2$ is greatly reduced than the regular ZSI.
Because the source current drawn is constant and continuous for the qZSI, it is more suitable for application in PV and fuel cells.

2.5.1 Circuit analysis of the Quasi-Z-Source Inverter(qZSI)

The Figure 2.10(a) shows the traditional voltage fed ZSI [13] and also the voltage fed qZSI respectively.

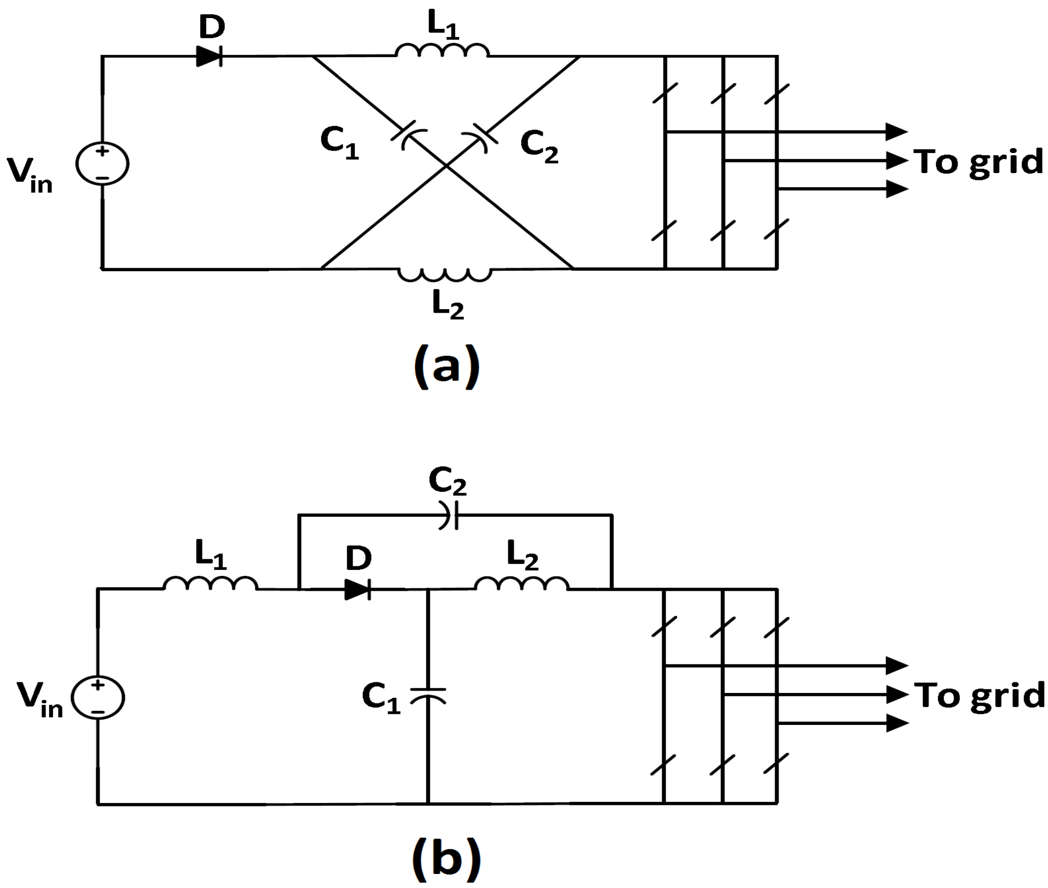

Figure 2.10: (a)Voltage fed ZSI and (b) Voltage fed qZSI.

As is the case with a regular ZSI, the qZSI also has two modes of operation i.e. the non shoot-through and the shoot-through mode. The effective equivalent circuit of a qZSI under the non shoot-through and shoot-through mode can be seen in the Figure 2.11. In the non shoot-through state of Figure 2.11(a), the inverter bridge/switches resemble a current source while the switches are shorted with V_{PN} equal to zero in the case of shoot-through state in Figure 2.11(b).

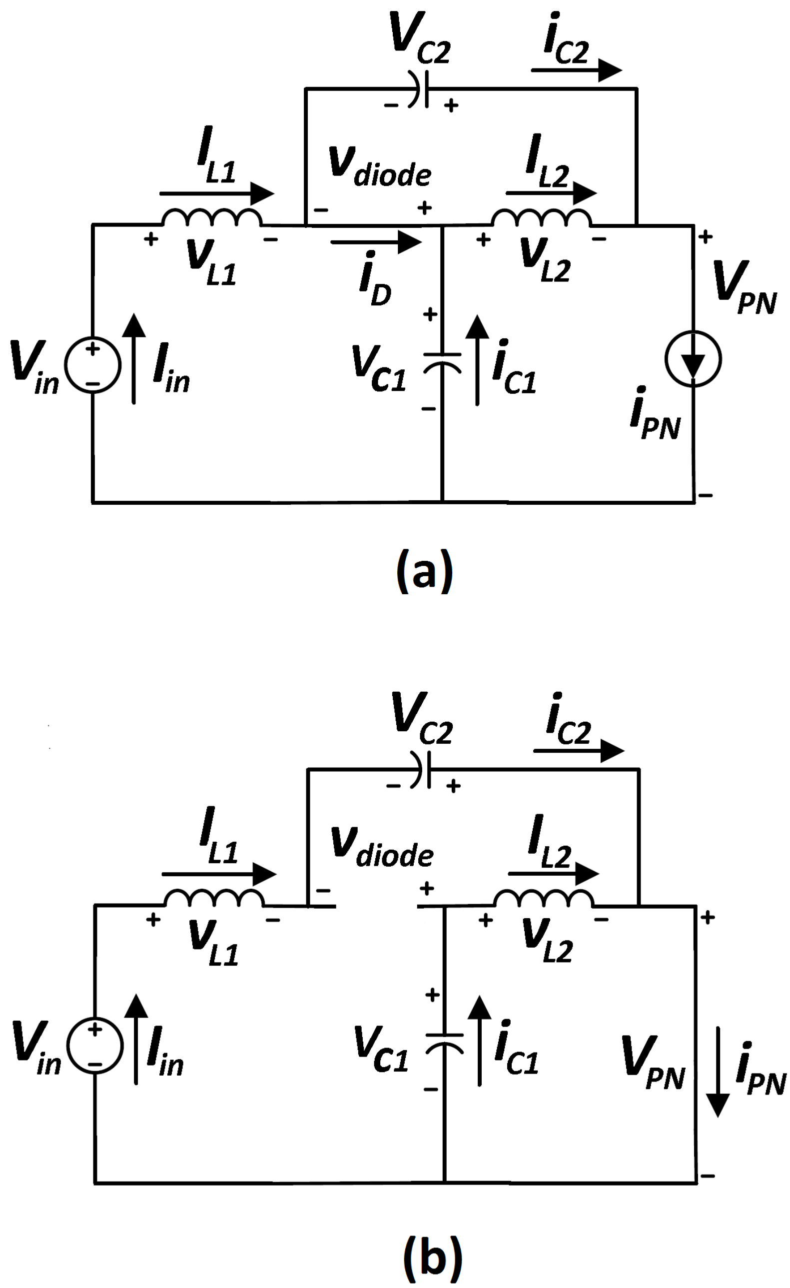

Figure 2.11: The qZSI equivalent circuit under (a) non-shoot-through and (b) shoot-through state.

The Figure 2.11 shows the voltage polarity and current flow directions. If the shoot-through interval is T_{sh} during a switching cycle of time period T then the shoot-through duty ratio is $D = T_{sh}/T$. Similarly the non shoot-through interval is $T_{nsh} = T - T_{sh}$. The Figure 2.11(a) shows a regular non shoot-through state for T_{nsh} time period, thus the inductor voltage for L_1 and L_2 shall be

$$v_{L1} = V_{in} - V_{C1}, \qquad \& \qquad v_{L2} = -V_{C2}, \tag{2.4}$$

Similarly for T_{nsh} the DC link and diode voltage V_{PN} and v_{diode} respectively are

$$V_{PN} = V_{C1} - v_{L2} = V_{C1} + V_{C2} \qquad \& \qquad v_{diode} = 0 \tag{2.5}$$

The Figure 2.11(b) reflects the current directions and voltage of the system for the shoot-through states T_{sh}, giving voltages

$$v_{L1} = V_{in} + V_{C2}, \qquad \& \qquad v_{L2} = V_{C1}, \tag{2.6}$$

Similarly for T_{sh} the DC link and diode voltage V_{PN} and v_{diode} respectively are

$$V_{PN} = 0 \qquad \& \qquad v_{diode} = V_{C1} + V_{C2} \tag{2.7}$$

Since the average of inductor voltage for a switching cycle is zero under steady state, from equation 2.4 and 2.6, we obtain

$$V_{L1} = \frac{T_{sh}(V_{in} + V_{C2}) + T_{nsh}(V_{in} - V_{C1})}{T} = 0 \tag{2.8}$$

$$V_{L2} = \frac{T_{sh}(V_{C1}) + T_{nsh}(-V_{C2})}{T} = 0 \tag{2.9}$$

Consequently,

$$V_{C1} = \frac{T_{nsh}}{T_{nsh} - T_{sh}} V_{in} \qquad \& \qquad V_{C2} = \frac{T_{sh}}{T_{nsh} - T_{sh}} V_{in} \tag{2.10}$$

The peak DC link voltage $\hat{V}_{PN}$ across the inverter bridge/switches can be found from the equations 2.5, 2.7 and 2.10 and comes out as

$$\hat{V}_{PN} = V_{C1} + V_{C2} = \frac{T_{nsh}}{T_{nsh} - T_{sh}} V_{in} = \frac{1}{1 - 2(T_{sh}/T)} V_{in} = BV_{in} \tag{2.11}$$

where B is the boost factor of the qZSI. If the system power rating is assumed P then we can calculate the average current across inductors L_1, L_2 as

$$I_{L1} = I_{L2} = I_{in} = P/V_{in} \tag{2.12}$$

Using Kirchhoff's current law and the equation 2.12 for capacitor and diode current, we get

$$I_{C1} = I_{C2} = I_{PN} - I_{L1} \qquad \& \qquad I_D = 2I_{L1} = I_{PN} \tag{2.13}$$

Based upon above equations and the equivalent circuit diagram, we can safely ascertain that the qZSI inherits all the advantages of ZSI. Infact, the qZSI has advantages over ZSI itself. Like ZSI, qZSI can buck-boost the input voltage and is more reliable than the traditional VSI based on the comparison drawn in Table 2.1.

2.6 Modeling of voltage fed Quasi-Z-Source Inverter(qZSI)

2.6.1 The steady state model of qZSI

The Figure 2.11 shows the equivalent circuit of the qZSI [14][15][16][18]. The qZSI inductor current directions and capacitor voltage polarity have also been shown in Figure 2.11. Henceforth, R denotes the series resistance of the capacitors and r denotes the parasitic resistance of the inductors while the L_f and C_f denote the filter values shown in Figure 3.9.

In the shoot-through state represented in the Figure 2.11(b), we can derive the circuit equations through the state-space equations, which are[34]

$$\begin{bmatrix} L_1 & 0 & 0 & 0 \\ 0 & L_2 & 0 & 0 \\ 0 & 0 & C_1 & 0 \\ 0 & 0 & 0 & C_2 \end{bmatrix} \begin{bmatrix} \dot{i}_{L1}(t) \\ \dot{i}_{L2}(t) \\ \dot{v}_{C1}(t) \\ \dot{v}_{C2}(t) \end{bmatrix} = \begin{bmatrix} -(R+r) & 0 & 0 & 1 \\ 0 & -(R+r) & 1 & 0 \\ 0 & -1 & 0 & 0 \\ -1 & 0 & 0 & 0 \end{bmatrix} \begin{bmatrix} i_{L1}(t) \\ i_{L2}(t) \\ v_{C1}(t) \\ v_{C2}(t) \end{bmatrix} + \begin{bmatrix} 1 & 0 \\ 0 & 0 \\ 0 & 0 \\ 0 & 0 \end{bmatrix} \begin{bmatrix} V_{in}(t) \\ I_{PN}(t) \end{bmatrix}$$

which is written as F$\dot{x}$=A$_1x + B_1u$.

In the non shoot-through state represented in the Figure 2.11(a), we can derive the circuit equations through the state-space equations, which are

$$\begin{bmatrix} L_1 & 0 & 0 & 0 \\ 0 & L_2 & 0 & 0 \\ 0 & 0 & C_1 & 0 \\ 0 & 0 & 0 & C_2 \end{bmatrix} \begin{bmatrix} \dot{i}_{L1}(t) \\ \dot{i}_{L2}(t) \\ \dot{v}_{C1}(t) \\ \dot{v}_{C2}(t) \end{bmatrix} = \begin{bmatrix} -(R+r) & 0 & -1 & 0 \\ 0 & -(R+r) & 0 & -1 \\ 1 & 0 & 0 & 0 \\ 0 & 1 & 0 & 0 \end{bmatrix} \begin{bmatrix} i_{L1}(t) \\ i_{L2}(t) \\ v_{C1}(t) \\ v_{C2}(t) \end{bmatrix} + \begin{bmatrix} 1 & R \\ 0 & R \\ 0 & -1 \\ 0 & -1 \end{bmatrix} \begin{bmatrix} V_{in}(t) \\ I_{PN}(t) \end{bmatrix}$$

which is written as F$\dot{x}$=A$_2x + B_2u$.

Now we have $A = D \cdot A_1 + (1 - D) \cdot A_2$ and $B = D \cdot B_1 + (1 - D) \cdot B_2$ obtained using the state space average method where D is the shoot-through duty cycle and $(1 - D)$ is the non shoot-through duty cycle.

Then we obtain

$$\mathrm{F}\dot{x}\mathrm{=Ax+Bu=}\begin{bmatrix} -(R+r) & 0 & D-1 & D \\ 0 & -(R+r) & D & D-1 \\ 1-D & -D & 0 & 0 \\ -D & 1-D & 0 & 0 \end{bmatrix}\begin{bmatrix} i_{L1}(t) \\ i_{L2}(t) \\ v_{C1}(t) \\ v_{C2}(t) \end{bmatrix} + \begin{bmatrix} 1 & (1-D)R \\ 0 & (1-D)R \\ 0 & D-1 \\ 0 & D-1 \end{bmatrix}\begin{bmatrix} V_{in}(t) \\ I_{PN}(t) \end{bmatrix}$$

If the system is in steady state then AX+BU=0 where X=$[I_{L1}\ \ I_{L2}\ \ V_{C1}\ \ V_{C2}]^T$, U=$[V_{in}\ \ I_{PN}]^T$.

That is

$$\begin{cases} -(R+r)I_{L1} + (D-1)V_{C1} + DV_{C2} + V_{in} + (1-D)RI_{PN} = 0 \\ -(R+r)I_{L2} + (D-1)V_{C2} + DV_{C1} + (1-D)RI_{PN} = 0 \\ (1-D)I_{L1} - DI_{L2} + (D-1)I_{PN} = 0 \\ (1-D)I_{L2} - DI_{L1} + (D-1)I_{PN} = 0 \end{cases}$$

Upon solving we get,

$$\begin{cases} V_{C1} = \frac{1-D}{1-2D}V_{in} - V_{22} \\ V_{C2} = \frac{D}{1-2D}V_{in} - V_{22} \\ I_{L1} = I_{L2} = \frac{1-D}{1-2D}I_{PN} \end{cases}$$

where,

$$V_{22} = \frac{(1-D)(R+2DR)}{(1-2D)^2}I_{PN} \tag{2.14}$$

We can see that the current in the two inductors is same for qZSI under steady state. If we ignore the series resistance R and parasitic inductance r, the V_{22} becomes zero. It can be seen in equation 2.14. On putting V_{22} equal to zero , we get

$$V_{C1} = \frac{1-D}{1-2D}V_{in} \qquad \& \qquad V_{C2} = \frac{D}{1-2D}V_{in} \tag{2.15}$$

2.6.2 The small signal model of qZSI

The small perturbation of state variables can be mathematically denoted as $\hat{x} = [_{L1}(t) \quad _{L2}(t) \quad \hat{v}_{C1}(t) \quad \hat{v}_{C2}(t)]^T$, whereas the input signals can be denoted as $\hat{u} = [\hat{V}_{in}(t) \quad \hat{I}_{PN}(t)]^T$ and shoot-through duty ratio is denoted by $\hat{d}(t)$.

If we put the above perturbed variables into F$\dot{x}$=Ax+Bu[17], we get small-signal state equations given below

$$\mathrm{F}\hat{\dot{x}}\mathrm{=Ax+Bu+}[(\mathrm{A}_1 - A_2) \cdot X + (B_1 - B_2) \cdot U] \cdot \hat{d} =$$

$$\begin{bmatrix} -(R+r) & 0 & D-1 & D \\ 0 & -(R+r) & D & D-1 \\ 1-D & -D & 0 & 0 \\ -D & 1-D & 0 & 0 \end{bmatrix} \begin{bmatrix} \hat{i}_{L1}(t) \\ \hat{i}_{L2}(t) \\ \hat{v}_{C1}(t) \\ \hat{v}_{C2}(t) \end{bmatrix} + \begin{bmatrix} 1 & (1-D)R \\ 0 & (1-D)R \\ 0 & D-1 \\ 0 & D-1 \end{bmatrix} \begin{bmatrix} V_{in}(t) \\ I_{PN}(t) \end{bmatrix} + \begin{bmatrix} V_{C1}+V_{C2}-I_{PN}R \\ V_{C1}+V_{C2}-I_{PN}R \\ -I_{L1}-I_{L2}+I_{PN} \\ -I_{L1}-I_{L2}+I_{PN} \end{bmatrix} \cdot \hat{d}(t)$$

Let $I_{11} = I_{PN} - 2I_L$, $V_{11} = V_{C1} + V_{C2} - I_{PN}R$ in the above matrix. Upon applying Laplace transforms to the state equations, they are converted into

$$sL_1\hat{i}_{L1}(s) = -(R+r)\hat{i}_{L1}(s)+(D-1)\hat{v}_{C1}(s)+D\hat{v}_{C2}(s)+\hat{V}_{in}(s)+(1-D)R\hat{I}_{PN}(s)+V_{11}\hat{d}(s) \tag{2.16}$$

$$sL_2\hat{i}_{L2}(s) = -(R+r)\hat{i}_{L2}(s) + D\hat{v}_{C1}(s) + (D-1)\hat{v}_{C2}(s) + (1-D)R\hat{I}_{PN}(s) + V_{11}\hat{d}(s) \tag{2.17}$$

$$sC_1\hat{v}_{C1}(s) = (1-D)\hat{i}_{L1}(s) - D\hat{i}_{L2}(s) + (D-1)\hat{I}_{PN}(s) + I_{11}\hat{d}(s) \tag{2.18}$$

$$sC_2\hat{v}_{C2}(s) = -D\hat{i}_{L1}(s) + (1-D)\hat{i}_{L2}(s) + (D-1)\hat{I}_{PN}(s) + I_{11}\hat{d}(s) \tag{2.19}$$

Now, for the sake of simplicity we assume $L_1 = L_2 = L$ and $C_1 = C_2 = C$(though C_2 is far less than C_1, we subtract equation 2.17 from 2.16 and equation 2.19 from 2.18 to get

$$\hat{i}_{L1}(s) - \hat{i}_{L2}(s) = \frac{sC}{LCs^2 + (R+r)Cs + 1} \cdot \hat{V}_{in}(s) \tag{2.20}$$

$$\hat{v}_{C1}(s) - \hat{v}_{C2}(s) = \frac{1}{LCs^2 + (R+r)Cs + 1} \cdot \hat{V}_{in}(s) \tag{2.21}$$

When we compare the equations 2.14 and 2.20, it is obvious that the inductor currents, i_{L1} and i_{L2} are different in small perturbation models which shows the difference in their dynamics[18]. Using equations 2.16 to 2.19, a signal flow graph of qZSI can be obtained as shown in the Figure 2.12.

The signal flow graph helps in deducing the transfer functions in equation 3.4 and 3.5 using Mason's gain formula.

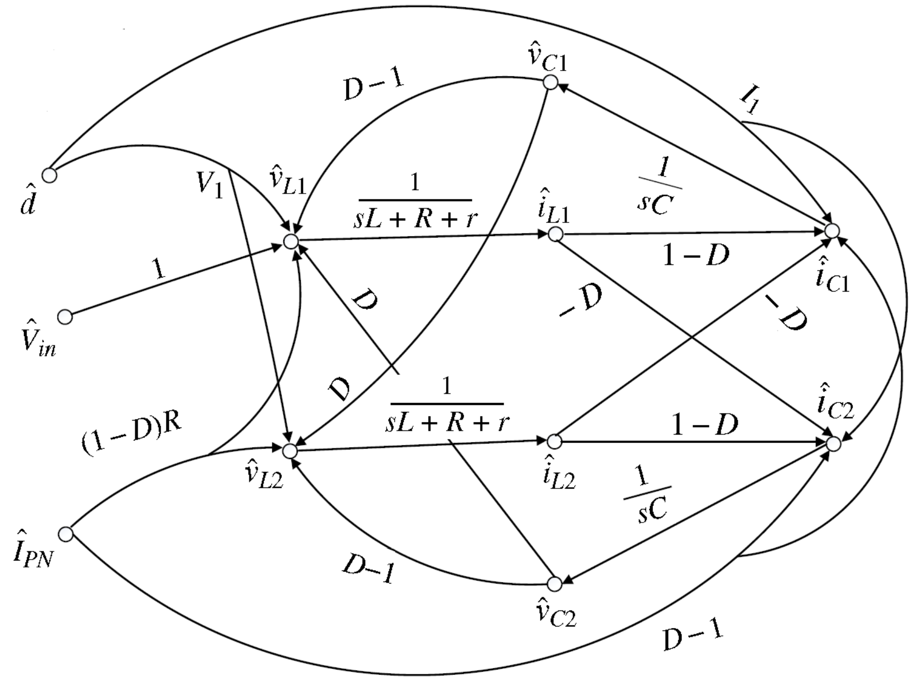

Figure 2.12: Signal flow graph used to obtain transfer functions in equation 3.4 and 3.5 [18].

The small-signal transfer functions of V_{C1} and i_{L2}[18] are obtained as below from the signal flow graph in above Figure 2.12.

$$\hat{v}_{C1}(s) = \frac{T_1(D-1) + (1-2D)(1-D)}{(T_1+1)[T_1+(1-2D)^2]} \cdot \hat{V}_{in}(s) + \frac{(1-2D)(1-D)R + T_2(1-D)}{T_1+(1-2D)^2} \cdot \hat{I}_{PN}(s) + \frac{(1-2D)V_{11} + T_2 I_{11}}{T_1+(1-2D)^2} \cdot \hat{d}(s) \tag{2.22}$$

$$\hat{i}_{L2}(s) = \frac{2T_1 D(1-D)}{T_2(T_1+1)[T_1+(1-2D)^2]} \cdot \hat{V}_{in}(s) + \frac{T_2(1-D)(1-2D) + T_1 R(1-D)}{T_2[T_1+(1-2D)^2]} \cdot \hat{I}_{PN}(s) + \frac{T_2(1-2D)I_{11} + T_1 V_{11}}{T_2[T_1+(1-2D)^2]} \cdot \hat{d}(s) \tag{2.23}$$

where $T_1 = LCs^2 + (R+r)Cs$ and $T_2 = Ls + R + r$.

2.7 Type of control methods for shoot-through duty cycle

There are ways to develop closed loop control of the power electronics in the qZSI. It can be achieved using the state-space averaging model or small signal modelling can be done [19][20]. A small signal model has been used to generate the transfer functions and obtain the closed loop control parameters for the qZSI in this work. But there are a broad range of methods available for controlling the DC link voltage V_{PN} around a value so as to obtain a near stable AC voltage at inverter output. Since the input source is Photovoltaic (PV) array, it has voltage variation based primarily on the irradiation available at a place and other factors. For the type of PV array used in the reference model*, temperature is a factor affecting voltage output. For the sake of simplicity it has been assumed constant at standard 25° celsius.
For application in Simulink model of qZSI controller, it was realized that to use a double loop control with inner current loop and outer voltage loop controlling the shoot-through duty cycle is a better control strategy. There can be other control strategies which might provide far better results.

2.7.1 Closed loop control

In the below Figure 2.13 one of the approaches used for controlling the qZSI has been shown. It involves usage of DC link voltage V_{PN} in the outer PI loop [20]. Another variation in it is using the qZSI capacitor voltage v_{C1} which has been later used in the Simulink model of qZSI PI controller. There are other closed loop control methods as well such neural networks, model predictive control (MPC) and fuzzy control, etc. The Figure 2.16 shows the non-linear control methods available for qZSI control.

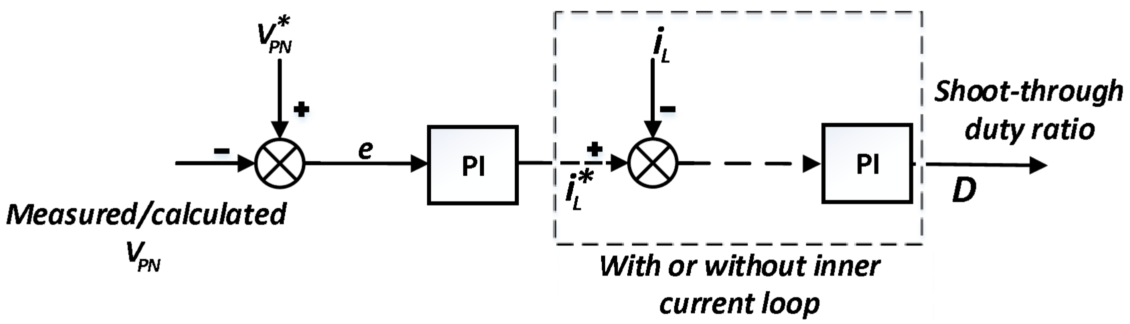

Figure 2.13: PI controller used to control the qZSI shoot-through duty ratio.

For the sake of understanding the control strategies, they have been divide into three main groups of closed loop control methods which are single loop, double loop and other advanced control methods.

2.7.1.1 Single control loop

In case of single loop controls the input voltage V_{in} [19], V_{C1} [21][22] or V_{PN} [23][24] is used as the feedback element to generate shoot-through duty ratio.

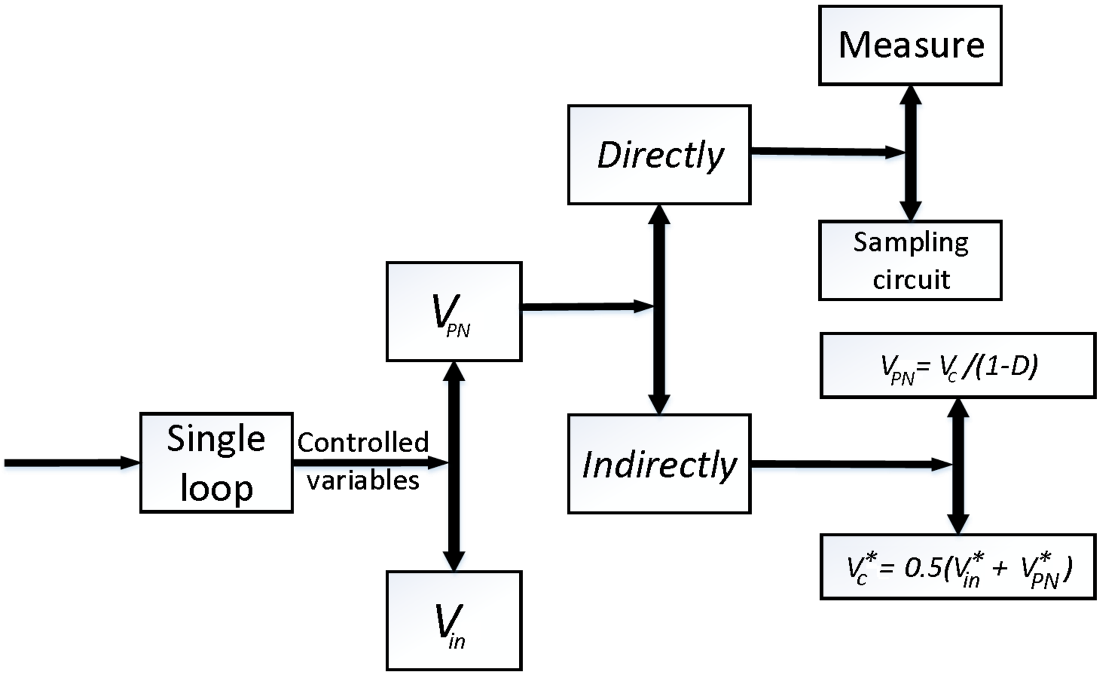

Figure 2.14: The various single loop controls for shoot-through duty ratio in qZSI.

The Figure 2.14 shows methods of controlling the qZSI using a single loop control method. The use of V_{PN} directly in the outer loop leads to complications owing to it being a pulsating signal varying between 620 ~640 V. The amount of variation in the pulses of V_{PN} is from a peak above 600V to all the way to 0V. Hence, instead of measuring V_{PN} directly [23] better control can be obtained by using a sampling circuit [25]. Another method is to utilize the indirect calculation of V_{PN} using the the qZSI capacitor voltage V_{C1} such that $V_{PN} = V_{C1}/(1\text{-D})$ [21], or $V_{C1}*=0.5(V_{in}*+V_{PN}*)$ [22].

However, the single-loop controls does not give a stable feedback controller owing to the non-minimum phase being a reason such that the DC link voltage changes with the variations in PV array voltage which in the qZSI Simulink model is sampled MPPT voltage.

2.7.1.2 Double control loops

In the Figure 2.15 below, the double loop block diagram shows presence of an inner inductor current i_{L2}, referred as i_L control loop with an outer DC link voltage V_{PN} control loop. The V_{PN} over here is again calculated indirectly as shown in above Figure 2.14 using the qZSI capacitor voltage V_{C1}. Because of the presence of a right half plane zero in the transfer function equation 3.4 shown later, non minimum phase presence is evident. Thus, a stable feedback controller can only be obtained with two loops such that the inner loop is comparatively very fast than the outer loop. The non minimum phase effects can be countered and qZSI system stability increased by using a P controller in the inner current loop [20]. A better stability margin is achievable with inclusion of an integrator as well inside the current control loop [26]. As stated earlier, in the controller design for the qZSI model, the simulation investigations of the double-loop control by outer PI controller and inner PI controller have been utilized.

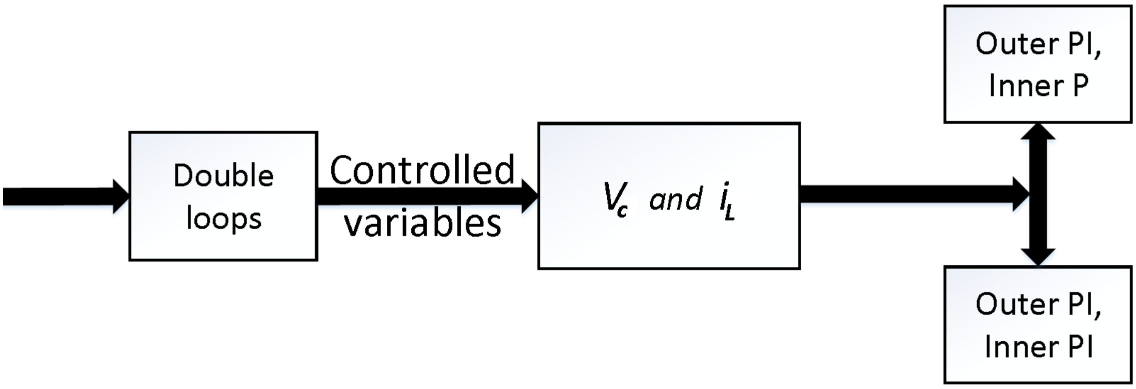

Figure 2.15: The double loop control methods for shoot-through duty ratio in qZSI.

2.7.1.3 Other control methods

As mentioned earlier, there can be another kind of qZSI controllers than the PI controllers mentioned in single loop methods. The below Figure 2.16 shows these methods. Non linear controllers such as fuzzy controller[27], neural network controller[28], sliding controller[29][30] and model predictive controller (MPC)[22] can also be used in qZSIs. The V_{in}, V_{PN}, i_L and V_{C1} serve as real time variables to generate the shoot-through duty cycle.

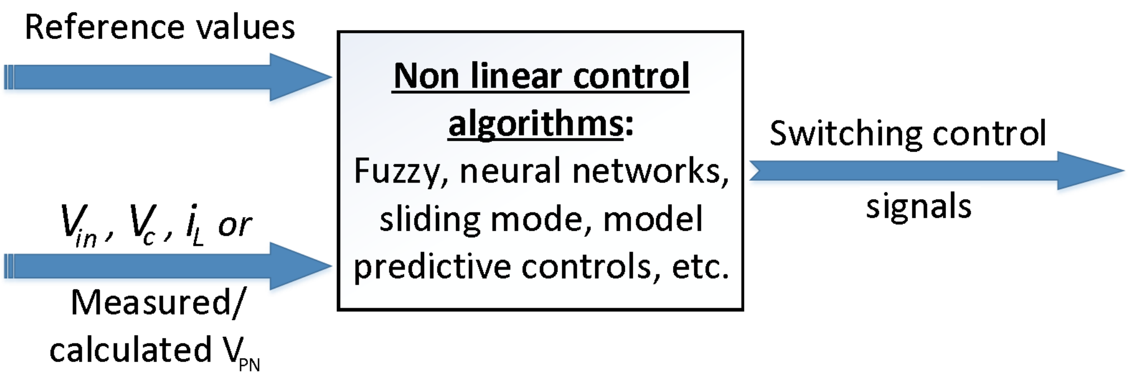

Figure 2.16: The non-linear control methods of shoot-through duty ratio in qZSI.

In comparison to regular controllers the advanced ones have faster responses yet the downsides prevent easier adoption. Their application is complex and tedious compared to the PI controllers which are readily used for the same processes.

3

Design of qZSI impedance network and controller

3.1 Designing qZSI impedance network

The impedance network of the qZSI is comprised of the capacitors C_1, C_2 and the inductors L_1, L_2. The carrier wave frequency is 10 kHz, so the shoot through frequency f_s for simple boost control method is twice of the carrier wave frequency, hence 20 kHz. Since the system operates in boost control mode for our application, we can calculate the maximum shoot through interval T_{0-max}

$$T_{0-max} = \frac{2 - \sqrt{3}M_{min}}{f_s} \tag{3.1}$$

The value of T_{0-max} is obtained as 26 μsec for M_{min}=0.85.
The function of the inductors in the impedance network of qZSI is to limit the ripple in the current during boosting. For convenience sake the inductance of L_1= L_2=L.

$$L = \frac{V_L \Delta T}{\Delta I} \tag{3.2}$$

The value of inductance is calculated as 300 μH. Upon simulation the value of inductance was varied and optimal value was found to be 100 μH and has been verified by pole-zero and bode plots.
Similarly the calculation of the capacitance value is also done. During the non shoot-through state the capacitors are in series. The function is to reduce the ripple content of voltage on the inverter bridge and consequently the harmonic distortion of the inverter output as well. The value of capacitors are not same but again for the sake of convenience the values of C_1 and C_2 are taken equal as C_1=C_2=C. It is to be noted that in case of ZSI the values of the capacitance C_1=C_2 and for inductance L_1= L_2. This is not the case in qZSI during practical conditions where the capacitance value C_2 is quite small compared to C_1. But in order to make the calculation and simulation easier, such an assumption has been taken here.

$$C = 2\frac{I_C \Delta T}{\Delta(V_{C1} + V_{C2})} = 300\mu F \tag{3.3}$$

One of the methods to optimize parameters is to use bode plots and determine the optimum value for the inductor L and capacitor C in impedance network.The inductance *L1* and *L2* of the impedance network are represented by L and similarly the capacitance *C1* and *C2* are represented by C henceforth. Also pole-zero maps can also be utilized for the same purpose. The transfer function in equation 3.4 is of utmost importance and is used for designing the DC side controller. It is of perturbations in capacitor voltage $\hat{v}_{c1}$ of the qZSI and the shoot-through duty ratio $\hat{d}$ derived from equation 2.22.

$$G_{V_{c1}d}(s) = \frac{\hat{v}_{c1}(s)}{\hat{d}(s)} = \frac{LI_1 s + (R+r)I_1 + (1-2D)V_1}{LCs^2 + (R+r)Cs + (1-2D)^2} \tag{3.4}$$

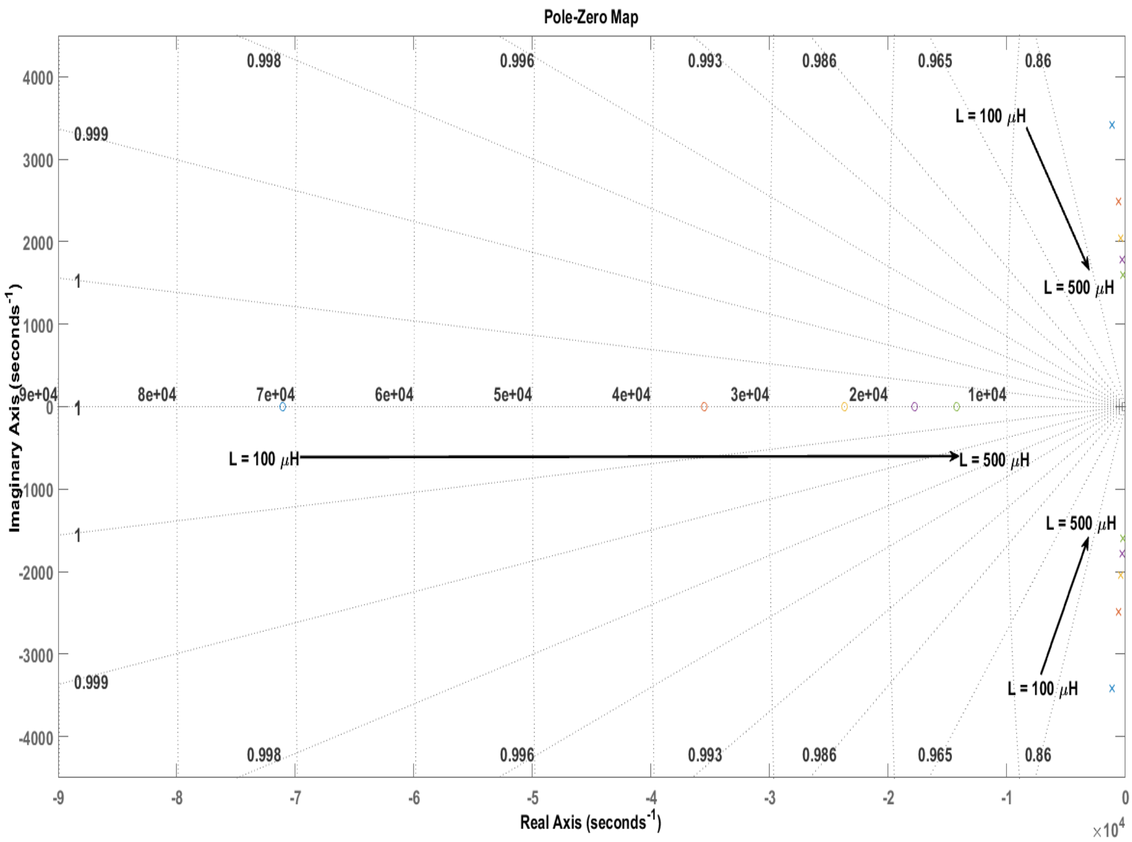

Figure 3.1: Changes in poles and zeros upon varying inductance with constant C=300 μF

The transfer function representing perturbations in inductor current $\hat{i}_{L2}$ and the shoot-through duty ratio $\hat{d}$ is as given in equation 3.5 below derived from equation 2.23 [18].

$$G_{i_{L2}d}(s) = \frac{\hat{i}_{L2}(s)}{\hat{d}(s)} = \frac{(Ls + R + r)(1-2D)I_1 + (LCs^2 + (R+r)Cs)V_1}{(LCs^2 + (R+r)Cs)[(Ls + R + r) + (1-2D)^2]} \tag{3.5}$$

In the above transfer function equations 3.4 and 3.5 , I_1=$I_{PN} - 2I_L$ and V_1 =V_{C1} +

$V_{C2} - I_{PN}R$, derived from Figure 2.11 where I_{L1} is taken equal to I_{L2} for simplicity.

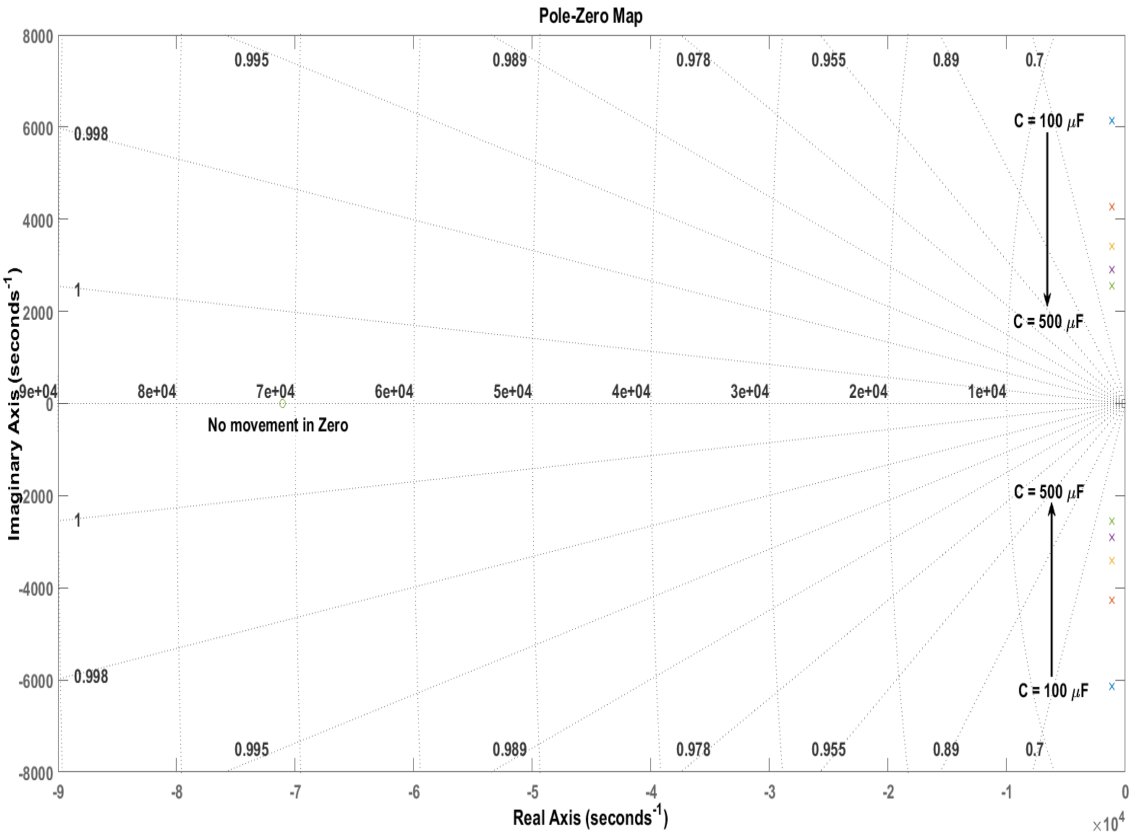

Figure 3.2: Changes in poles upon varying capacitance with constant L=100 μH

For optimising values of inductance L and capacitance C, both are varied with one kept constant at a time causing observational changes in the movement of poles and zeros. As and by the inductance L is increased from 100 μH to 500 μH in with capacitance constant at 300 μF the variation in zeros is from negative real axis towards the origin in Figure 3.1. This signifies an increase in the non-minimum phase undershoots, while the movement of poles increases the system settling time and response. The non-minimum phase undershoot occurs in a lot of converters and typically is recognized by an undershoot to a step response. In the second case when we start varying capacitance C from 100 μF to 500 μF, Figure 3.2 shows the shifting of poles vertically towards the real axis, while the zeros stay constant.

With the changes of L and C, the bode plots of the transfer function $G_{V_{C}d}$ are shown in Figure 3.3 and 3.4. It can be seen that when inductance increases, the amplitude–frequency characteristic changes gently and the quality factor decreases. However when the capacitance increases, the amplitude–frequency characteristic changes steeply and the quality factor increases. Similarly, the resonant frequency reduces with the two parameters increasing.

Thus, the optimised value of the inductance L and capacitance C were found to be 100 μ H 300 μ F respectively. The others values for filter and R and r have been optimised by simulations.

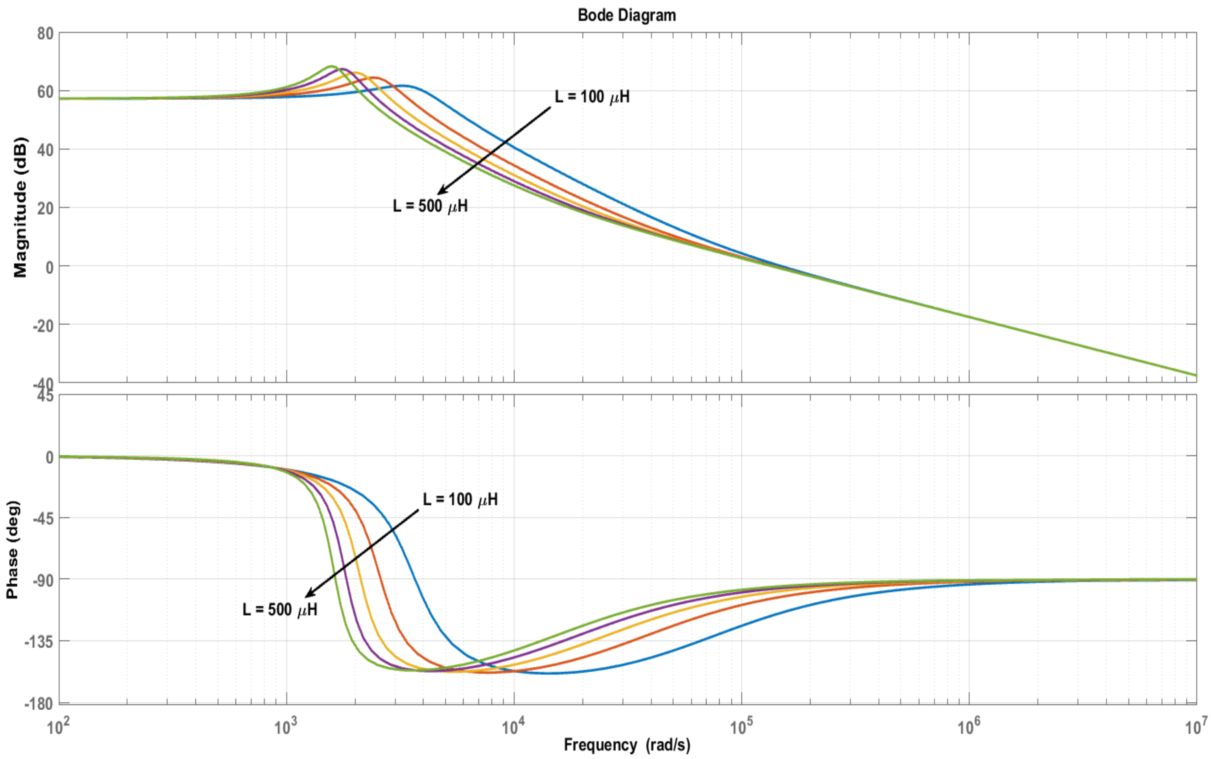

Figure 3.3: Bode plot for varying inductance and C=300 μF

The bode plots in Figure 3.3 & 3.4 for various values of L and C obtained by varying one and keeping the other constant at a time.

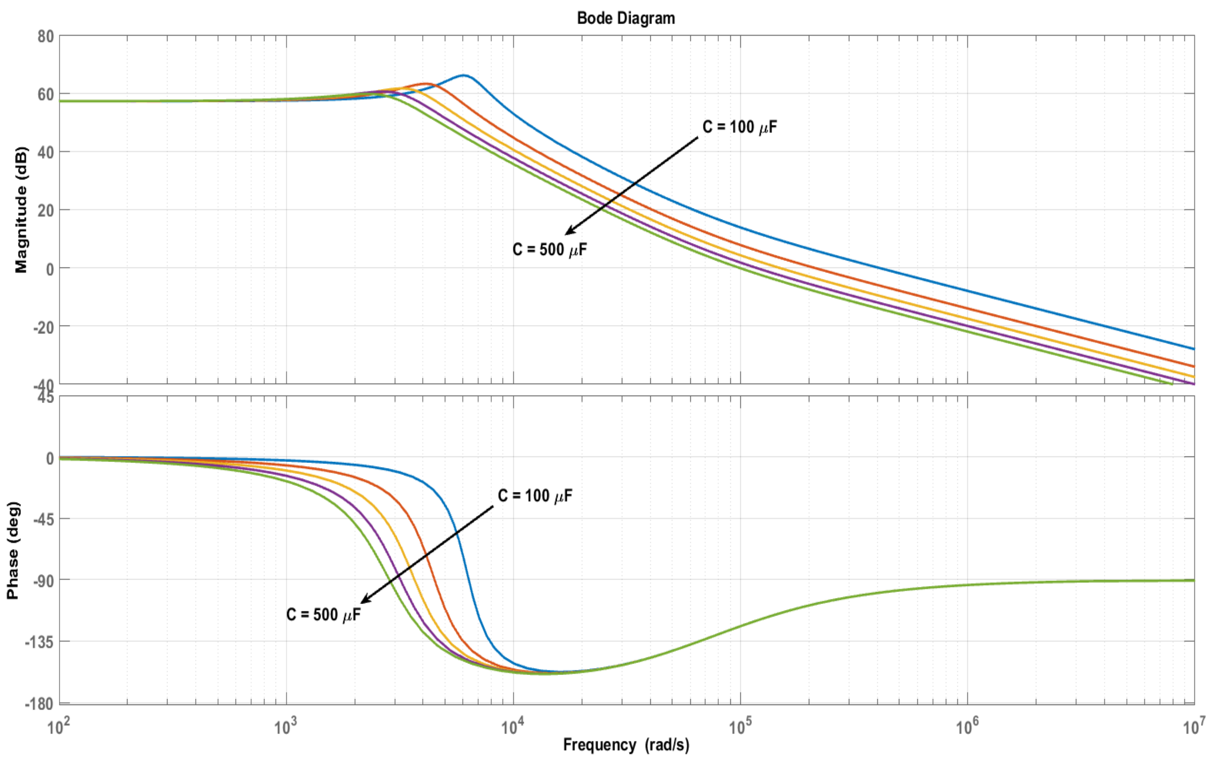

Figure 3.4: Bode plot for varying capacitance and L=100 μH

The values of the parameters used in Simulink model of the qZSI. The value of shoot-through duty cycle D has been calculated using the boost factor.

L=100 μH	C=300 μF
R=0.08 Ω	r=0.15 Ω
$L_f = 1000\mu H$	$C_f = 110\mu F$
$R_L = 5\Omega$	D=0.28

Table 3.1: Parameters used in Simulink qZSI model

3.2 Control strategy of qZSI

The main control strategies of qZSI are the following four[18]:

- Simple boost control,
- Maximum boost control[31],
- Maximum constant boost control[32],
- Modified space vector PWM (MSVPWM) control [34].

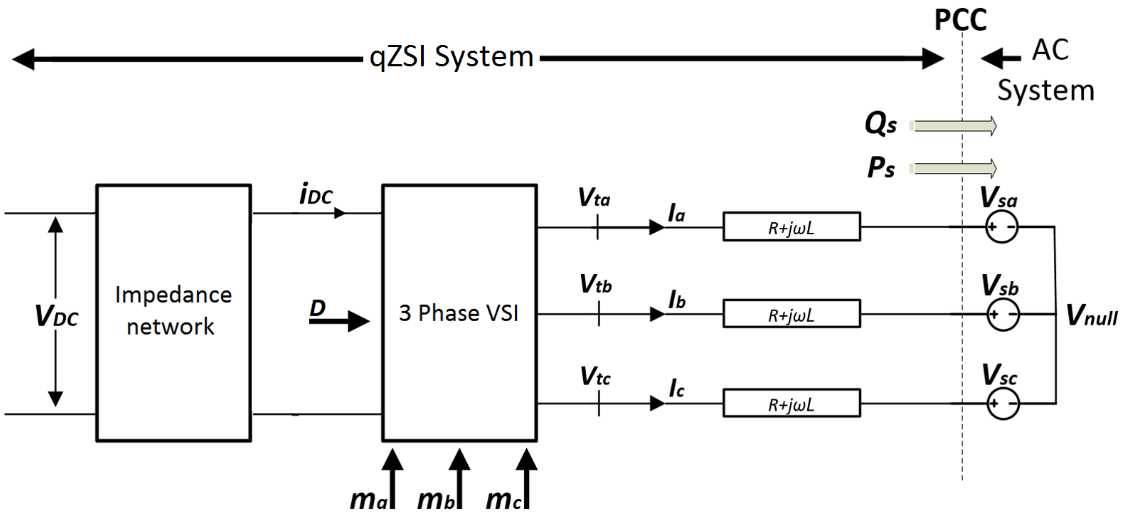

Figure 3.5: Implementation of a qZSI to grid connected PV arrays.

In the Simulink model of qZSI, the implementation of control strategy is similar to simple boost control since it is the simplest of all control strategies.

3.2.1 Sinusoidal PWM and shoot-through implementation

The Pulse width modulation(PWM) strategy used in simulating qZSI is sinusoidal PWM(SPWM). In SPWM a triangular carrier wave and sinusoidal reference waves are used for generating signal for switches of the inverter. These signals are generated by comparing the reference wave with the carrier wave. A high signal is generated for reference wave > carrier wave. Similarly, a low signal is generated for vice-versa. The shoot through state basically involves the switches being open for longer time period. This can be accomplished by generating high and low for it and supplying simulataneously with the SPWM.

The Figure 3.6 illustrates SPWM.

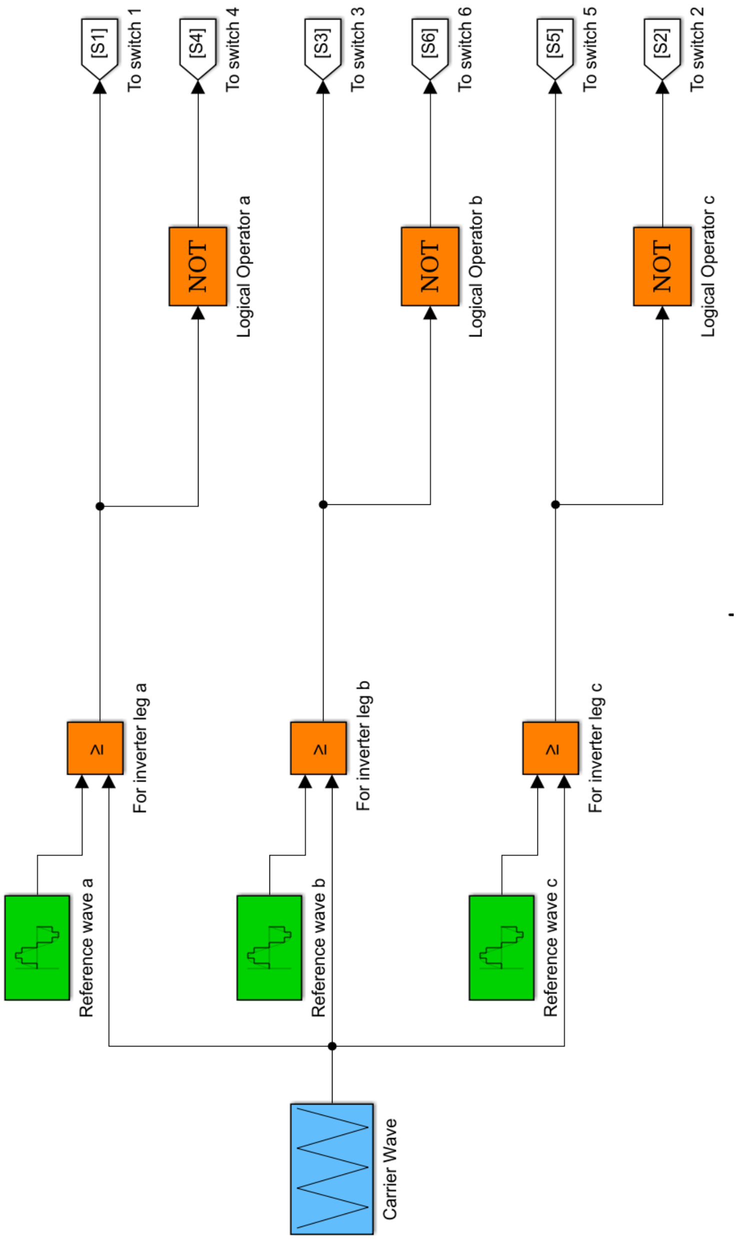

Figure 3.6: Sinusoidal PWM

The Figure 3.7 shows the Simulink block diagram of SPWM and shoot through signals supplied to the inverter switches .

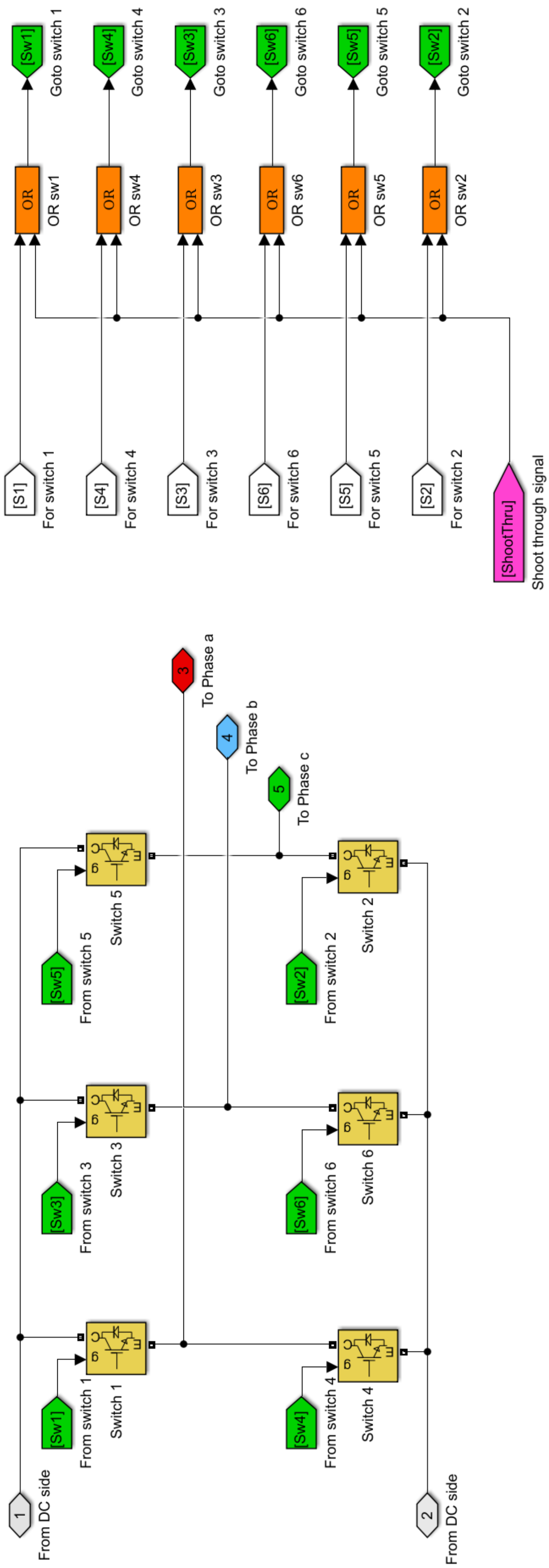

Figure 3.7: Sinusoidal PWM implementation in Simulink

3.3 DC side controller design for qZSI

3.3.1 Internal model control(IMC)

Controller design using the Internal Model Control(IMC) involves parameterization of the controller with respect to the plant model and the band width of the closed loop[33] as demonstrated in Figure 3.8 below.

$$i = G(s)u_s = G(s)F_c e = G(s)F_c(i_{ref} - i) \tag{3.6}$$

$$(1 + G(s)F_c(s))i = G(s)F_c(s)i_{ref} \tag{3.7}$$

$$\frac{i}{i_{ref}} = \frac{G(s)F_c(s)}{1 + G(s)F_c(s)} = G_{cl} = \frac{\alpha_c}{s + \alpha_c} = \frac{\alpha_c/s}{1 + \alpha_c/s} \tag{3.8}$$

$$G(s)F_c(s) = \frac{\alpha c}{s} \tag{3.9}$$

Thus, the controller transfer function $F_c(s)$ as shown in Figure 3.8 will come out to be

$$F_c(s) = \frac{\alpha_c}{s}G^{-1}(s) \tag{3.10}$$

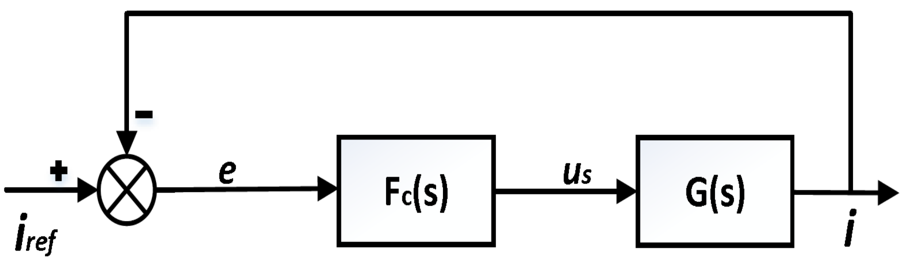

Figure 3.8: Closed loop representation of plant model $G(s)$ with controller transfer function $F_c(s)$.

3.3.2 Output saturation and anti-windup

The current loop although treated as linear and ideal system is actually far from it. The duty cycle has a limit to it since it can't be more than 1. Hence output saturation has to be prevented and also the system becoming non linear. The lower and upper limit set for saturation for duty cycle is 0.28-0.32 respectively and is arrived at using equation 2.11 for boost factor and duty cycle.

Anti-windup is employed to prevent an overshoot(to the step response) that occurs if integrator is fed very large error value. Since large error **e** can't be fed to the integrator, another error value $\hat{e}$ has to be given. Back-calculation and clamping

can be used to implement anti-windup.
The error signal **ê** fed to the integrator using back calculation method[33] is

$$\hat{e} = e + \frac{Output_{limted} - Output_{unlimited}}{K_p} \tag{3.11}$$

Both saturation and anti-windup are used only in the inner loop of the simulated qZSI Simulink model.

3.3.3 DC side controller

A block diagram representation of DC side controller[18] is shown in Figure 3.9 below. The relation between voltage V_{PN} and V_{C1} is derived using equation 2.11 and 2.15 and serves to calculate V_{PN} error for PI controller input. The inner control loop is used to generate the shoot-through duty ratio and then shoot-through pulses supplied along with those of SPWM to the inverter switches maintaining V_{PN} around $620 \sim 640V$.

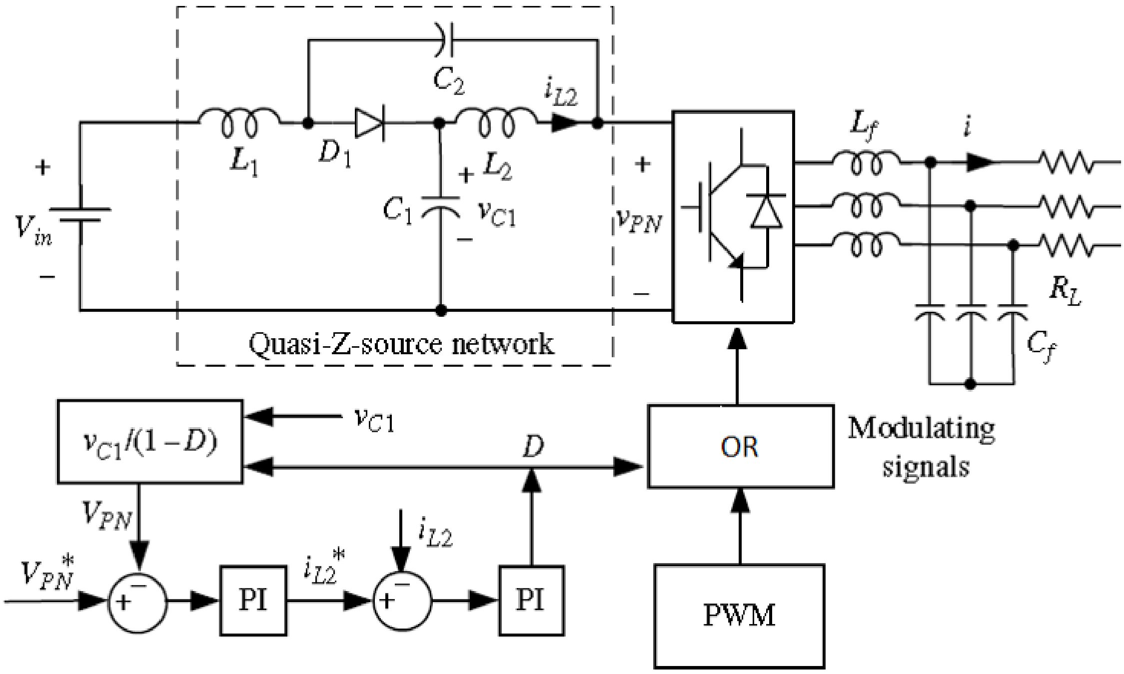

Figure 3.9: The DC side controller design with PI controller in the inner loop

Based on the above Figure 3.9(a) Simulink model has been made. The Figure 3.10 is qZSI model made in Simulink and used to compare with the reference model* of PV array connected VSI supplying power to the grid.
It is also compared with the solar inverter installed in Chalmers lab. The reference model* used for comparison with the qZSI Simulink model is shown in Figure 3.11. The reference model* is available in the Simulink library(power_PVarray_grid_det) and has been sufficiently modified to compare with the simulated qZSI model.

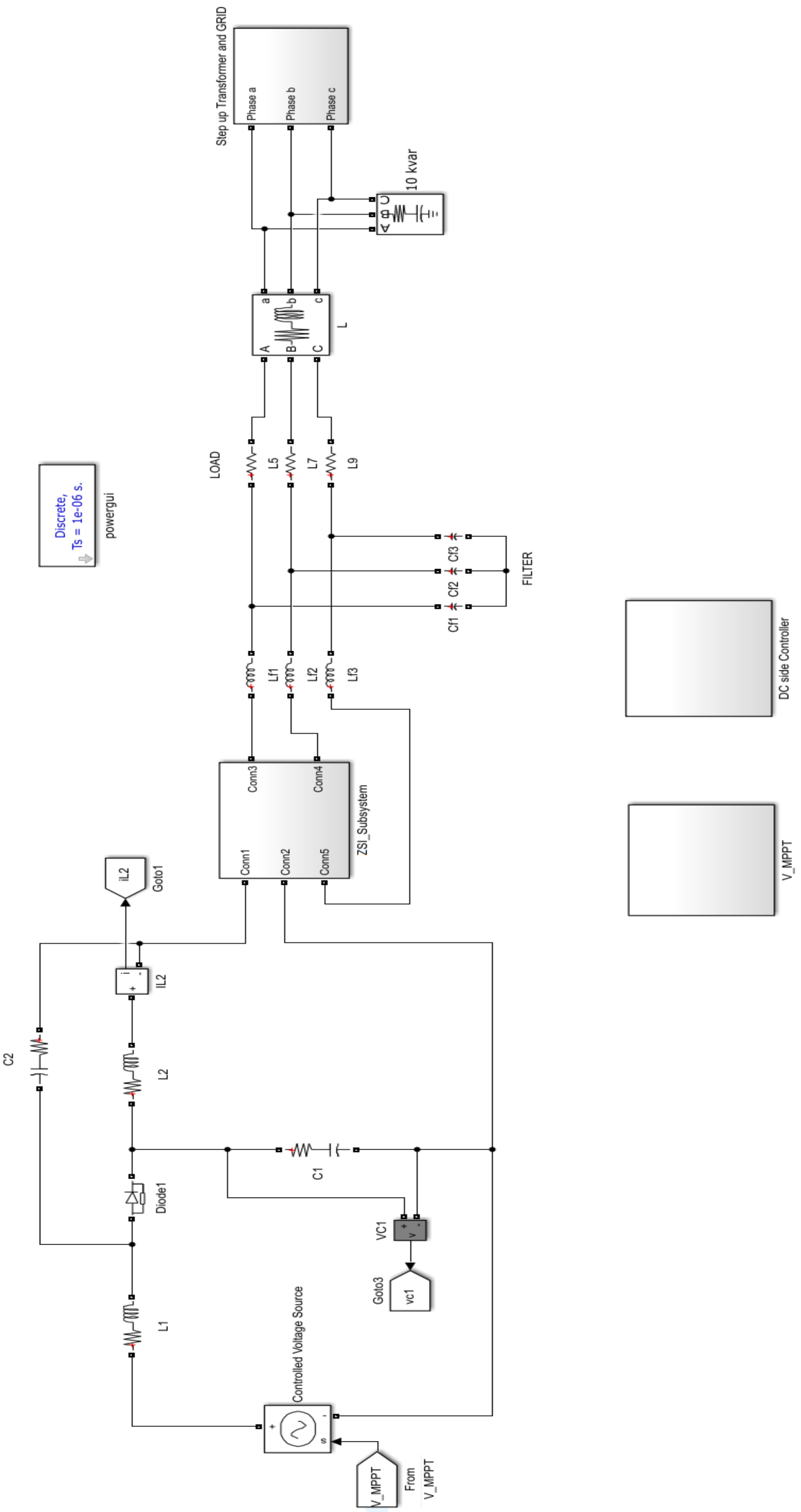

Figure 3.10: Simulink model of qZSI used to compare with the reference model*

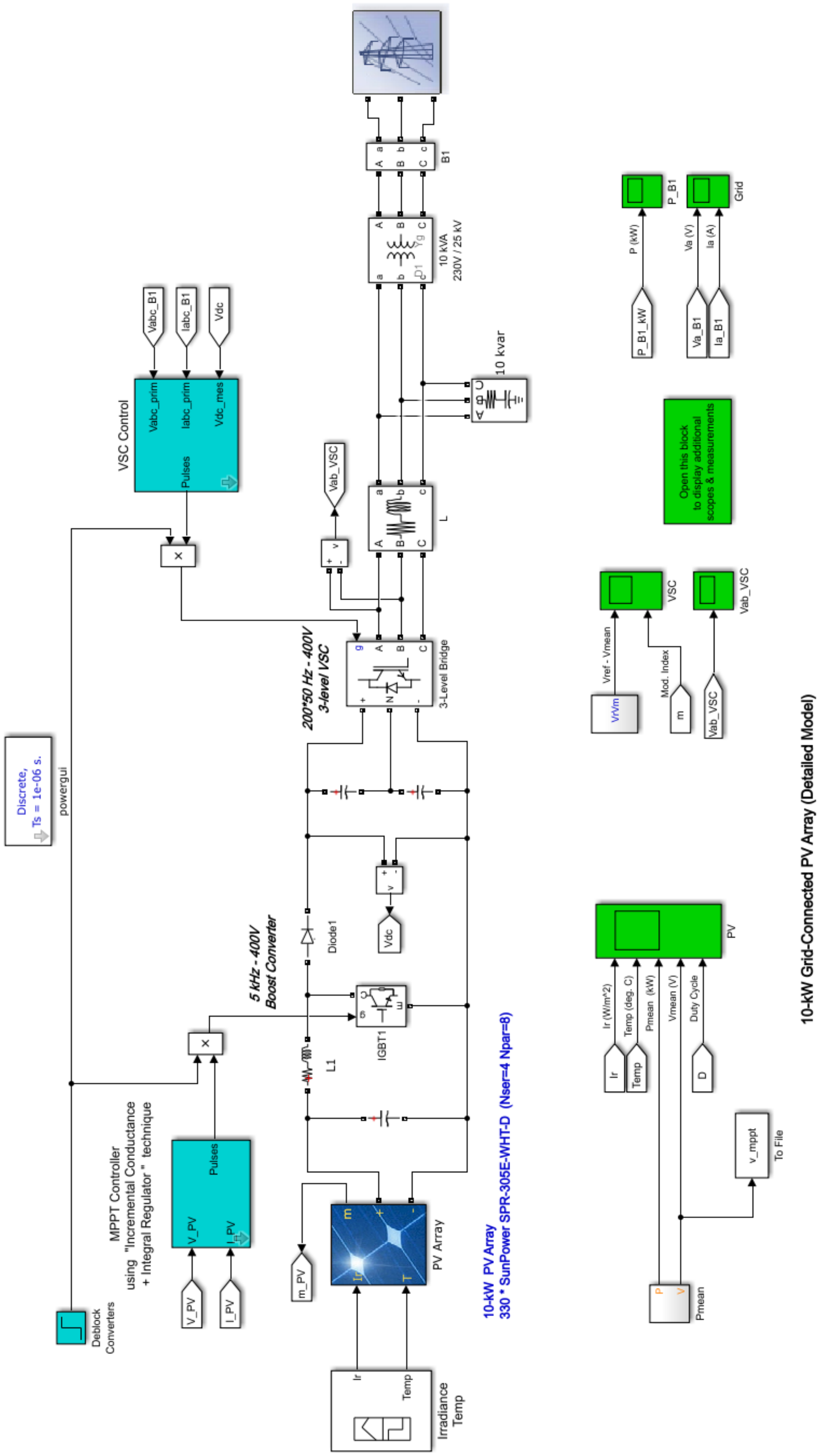

Figure 3.11: The reference model* available in Simulink library used for comparison with simulated qZSI model (power_PVarray_grid_det).

In order to keep the input same to the inverters, sampled MPPT voltage in Figure 3.12 was taken from the reference model* and it serves as qZSI model's input. The variation of MPPT voltage as shown in Figure 3.12 is found to be from 227 V to 321 V but under steady state it varies from 250 V to 273.5 V. The qZSI in simulation works in boost mode all the time, pumping up the voltage DC link voltage = V$_{DcLink}$ = V_{PN} to about 620 $\sim$ 640 V for most of the cycle of 1.2 *sec* to get an AC output of 230 Vpeak.

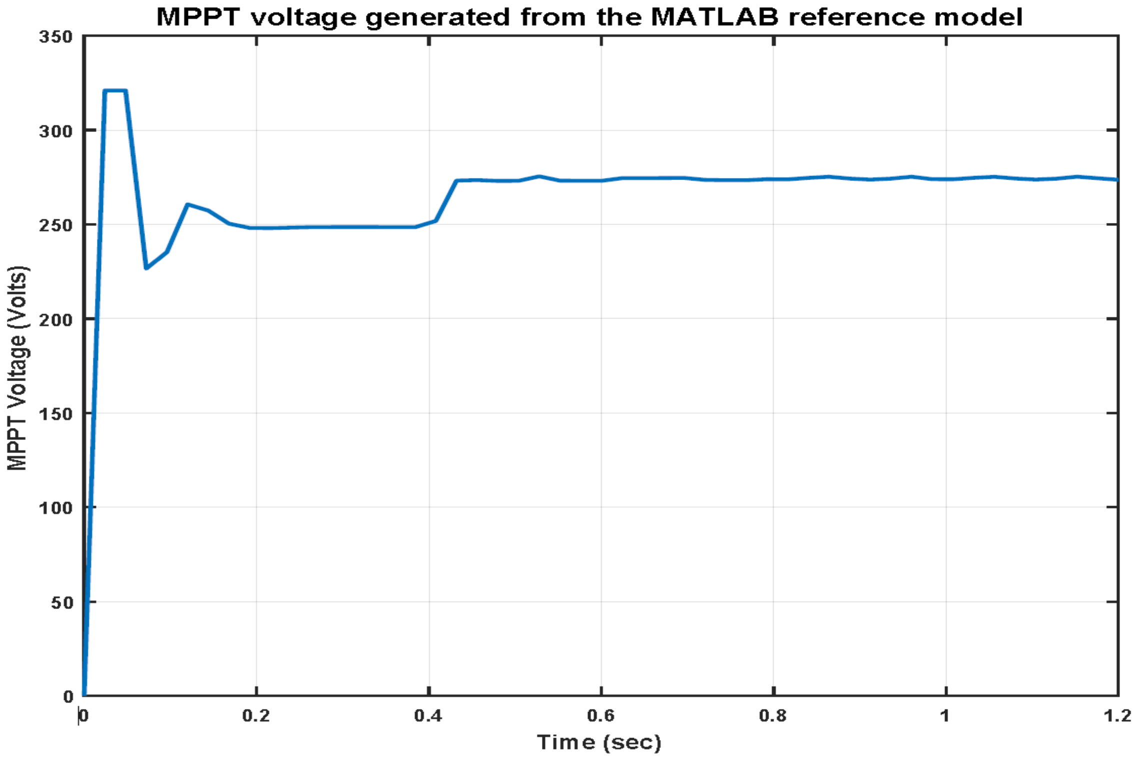

Figure 3.12: Sampled MPPT voltage from the reference model*

The DC side controller subsystem in the Figure 3.10 has been derived from the block diagram shown in Figure 3.13 below. It consists of two loops: the inner current loop and the outer voltage loop. PI controllers are used in both the loops.

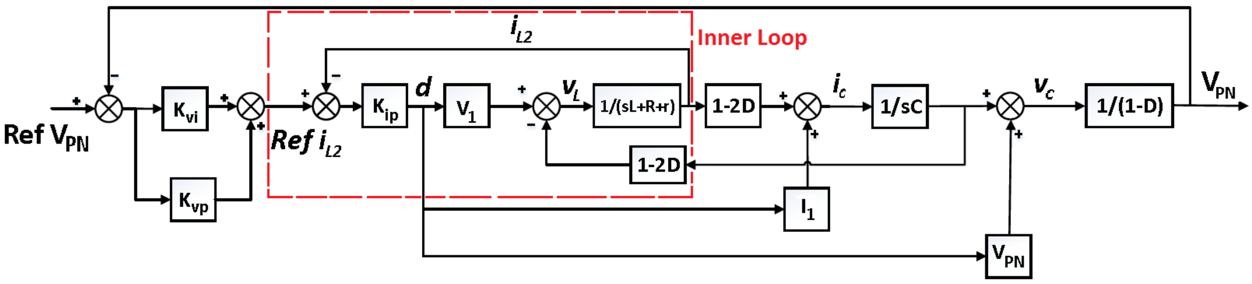

Figure 3.13: Block diagram representation of the closed loop

In the Figure 3.13, the inner loop is inductor $L2$ current loop and can be taken to be very fast compared to the outer loop and hence equal to 1. The outer loop represents the peak DC link voltage loop.

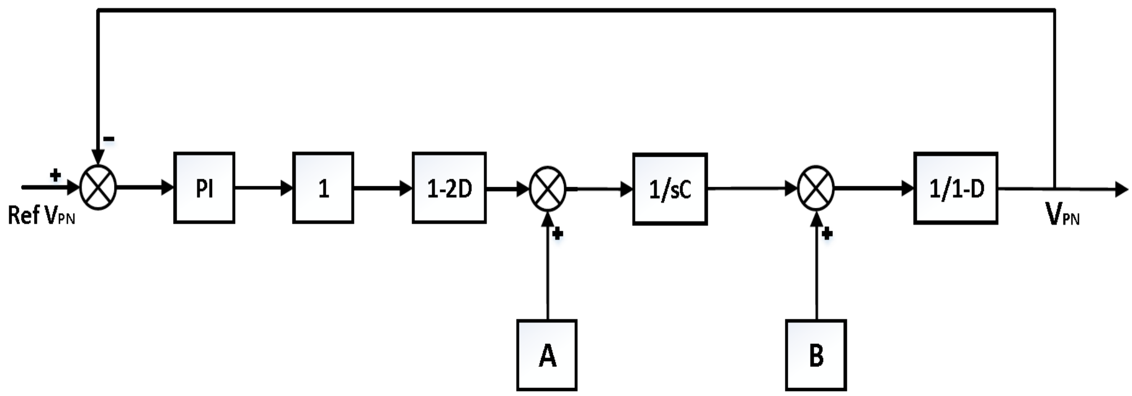

Figure 3.14: Simplified block diagram representation of the closed loop

The feed-forward product of I_1 and V_{PN} with d represented as A and B respectively in Figure 3.14 above can be sufficiently assumed to an average value based on the range of variation in duty cycle. Hence the terms are reduced into an average numerical value simplifying the block diagram. With this method the block diagram in Figure 3.13 was separated into distinct inner and outer loops. The closed loop transfer function for both the loops was obtained and then shaped to be a first order system with bandwidth α_i for inner loop.
The outer loop bandwidth α_v was chosen a decade smaller than the inner loop bandwidth α_i.

$$\alpha_v \leq \frac{\alpha_i}{10} \tag{3.12}$$

The outer loop transfer function was obtained from Figure 3.14 and PI controller values were calculated. The same process was repeated to obtain the inner loop transfer function and PI controller values. The controller values for both the inner and outer loop are shown in Table 3.2 below.

Outer Loop	**Inner Loop**
$K_{pv} = 18$	$K_{pi} = 8.2e^{-3}$
$K_{iv} = 2.3$	$K_{ii} = 6.3$

Table 3.2: PI controller parameters for separate inner and outer loop

The step responses of the inner and outer loop are shown in Figures 3.15 and 3.16 respectively. Important point to be note is the separation of inner and outer loops done and PI controller values calculated. But eventually, these values were fed into the cascaded PI controllers of inner and outer loop which lead to different values of PI controller upon tuning further. The values of PI controller for cascaded case are as shown in Table 3.3 which were fed in the DC side controller subsystem in Figure 3.10.

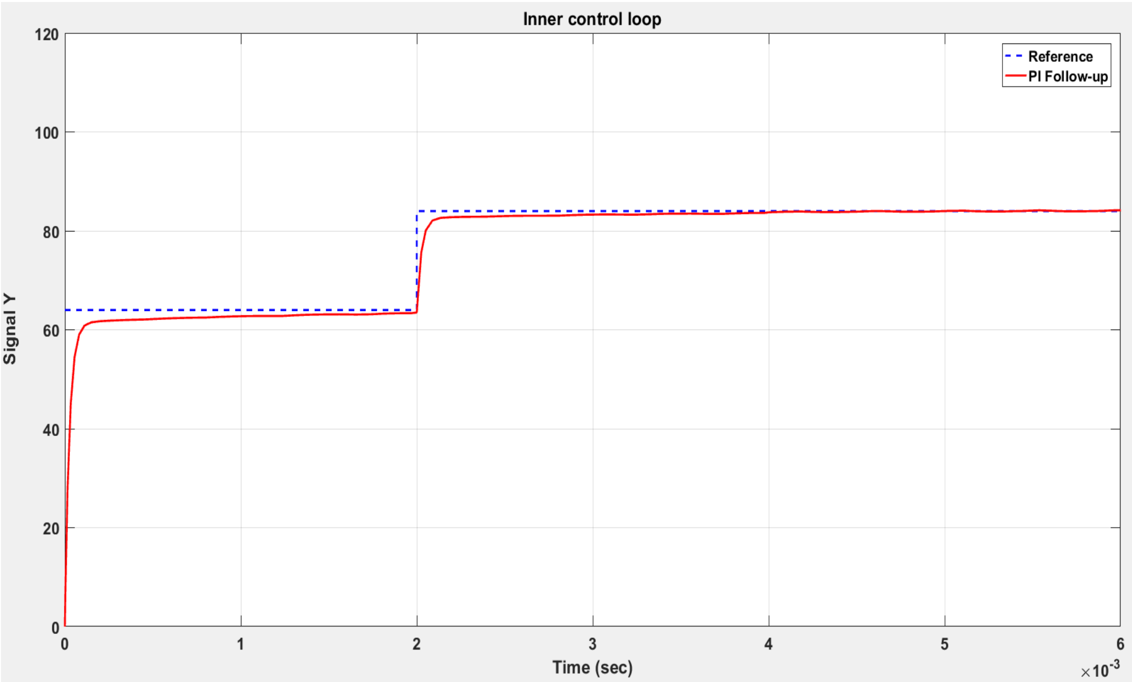

Figure 3.15: PI response to the inner control loop

The controller response to step inputs is shown in Figures 3.15 and 3.16.

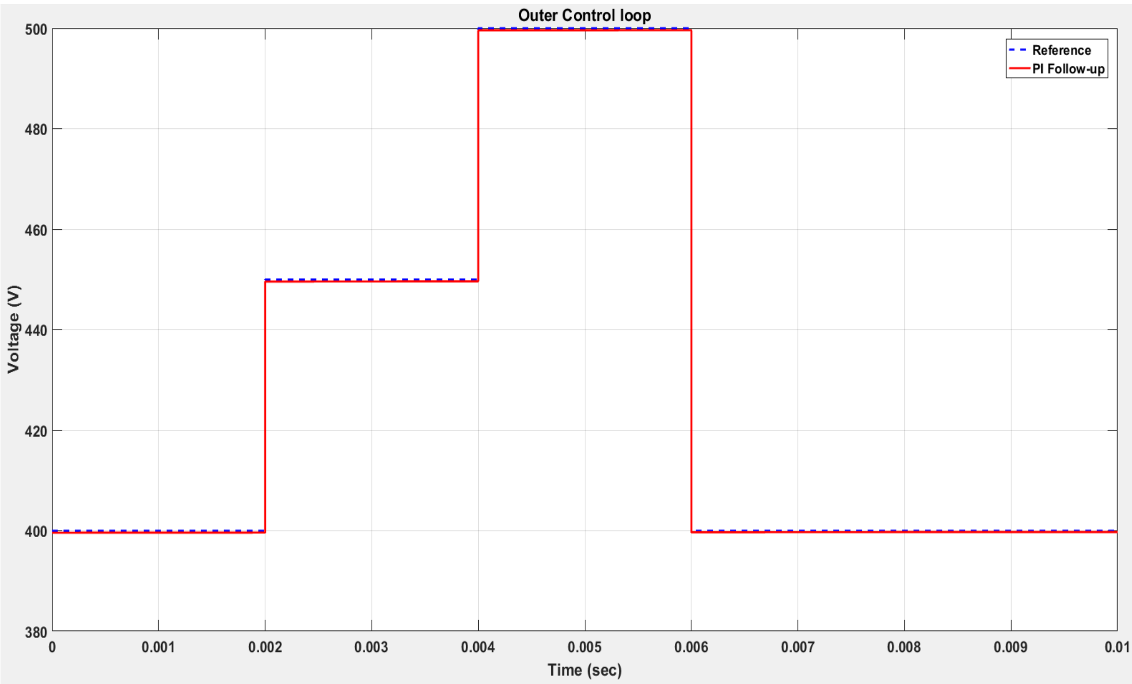

Figure 3.16: PI response to the outer control loop

The values in the Table 3.3 below have been used in the final Simulink model of qZSI with DC side controller, that was compared with the reference model*.

Outer Loop	**Inner Loop**
$K_{pv} = 0.18$	$K_{pi} = 8.2e^{-3}$
$K_{iv} = 80$	$K_{ii} = 10$
$\alpha_v = 100\pi$	$\alpha_i = 1000\pi$

Table 3.3: PI controller parameters for cascaded inner and outer loop

4

Results and Discussion

4.1 Results

The qZSI simulation was run and the plots obtained were compared with the plots generated using the reference model* of VSI. The DC link voltage V_{PN} plot is shown in the Figure 4.1 below. The voltage V_{PN} during the major part of the first 0.2 sec has sharp variations which are caused by similar variations in the input MPPT voltage (sampled from the reference model*) in Figure 3.12. For the rest of the duration the V_{PN} varies from 620V $\sim 640V$.

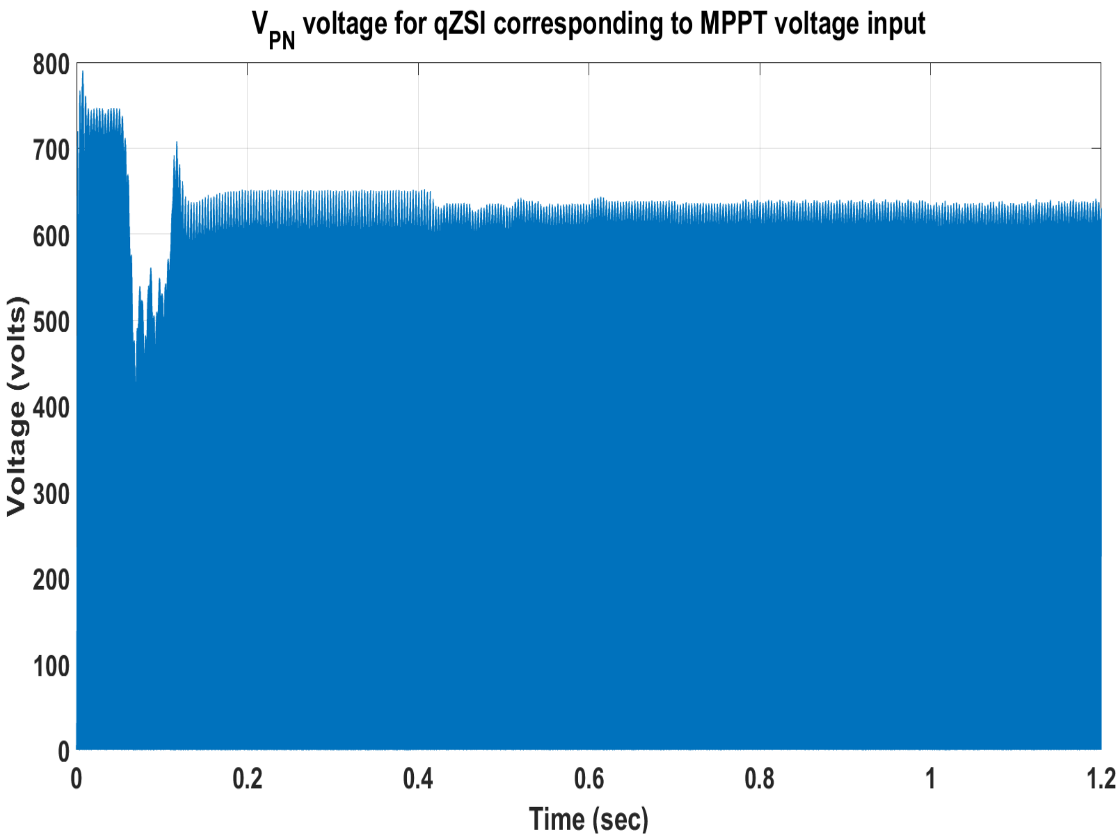

Figure 4.1: V_{PN} voltage at qZSI

Corresponding to the DC link voltage V_{PN}, the voltage on the AC side is observed to stay close to 230 V in Figure 4.2 with no considerable variations upon change in the input MPPT voltage in Figure 3.12. The current in phase 'a' of three phases also stays almost constant with minute variations around 45A $\sim 46A$.

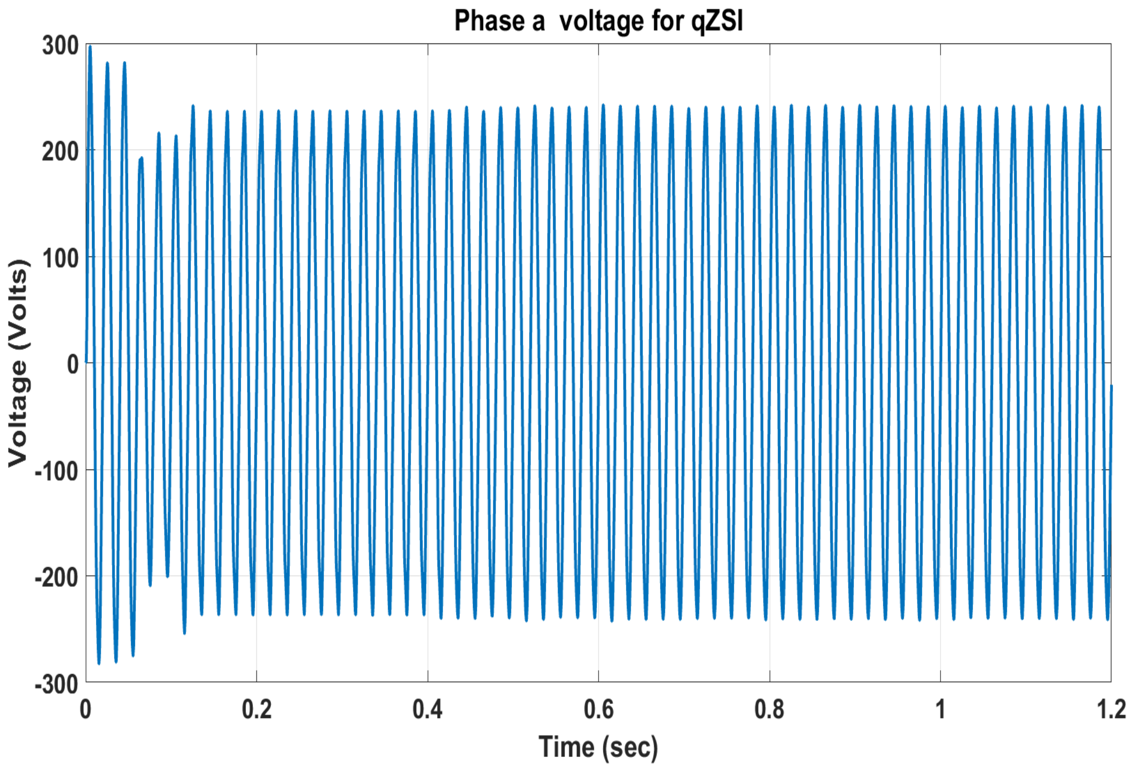

Figure 4.2: Output voltage in phase 'a' of simulated qZSI model

The Figure 4.2 and 4.3 show output voltage and current respectively in phase 'a'.

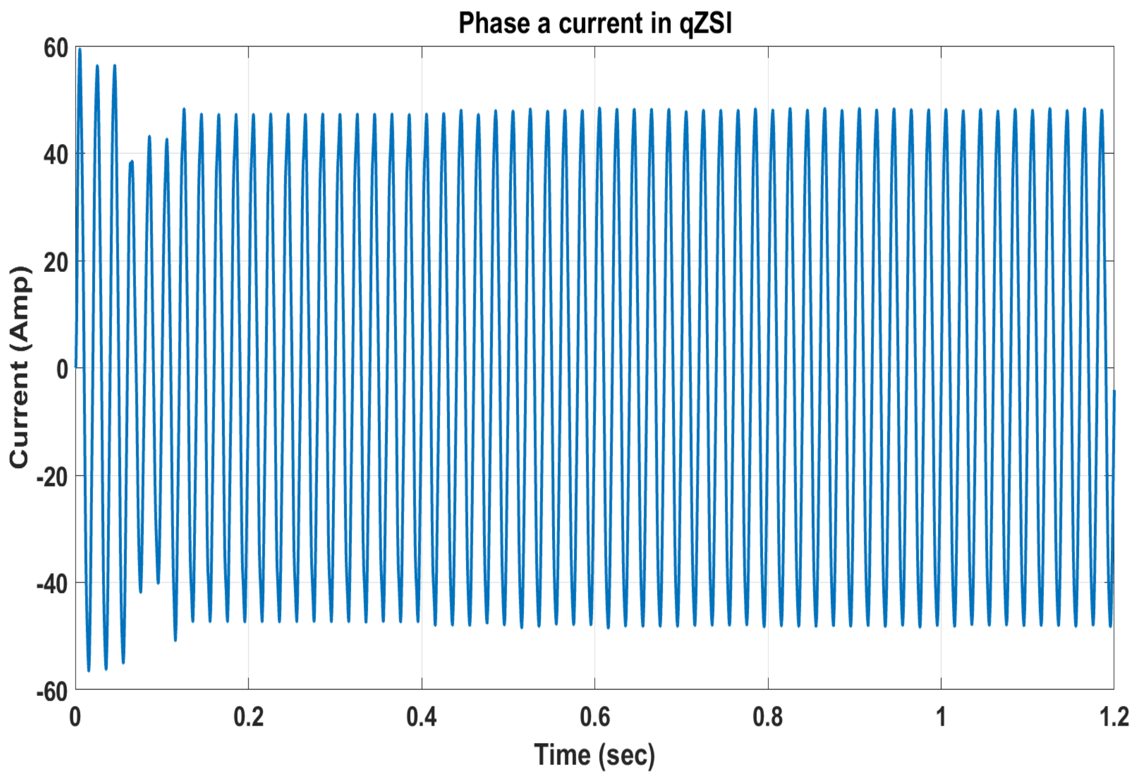

Figure 4.3: Output current in phase 'a' of simulated qZSI model

The shoot-through duty cycle value varies from 0.28 to 0.32.

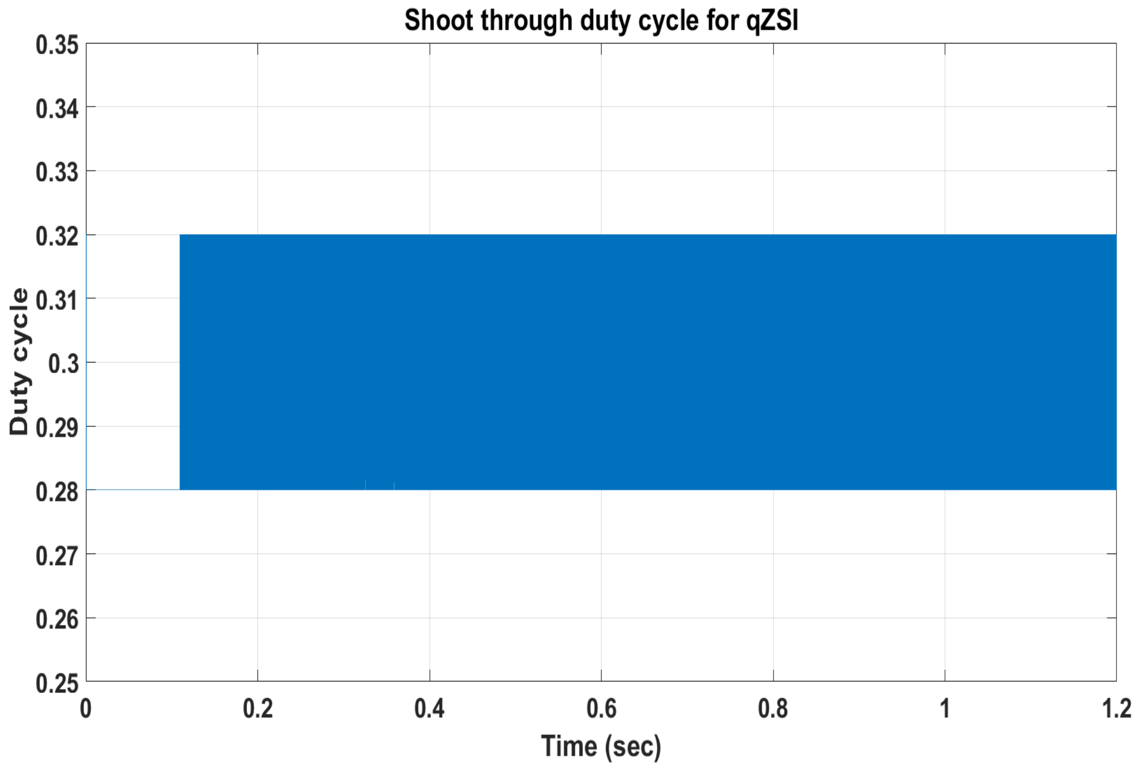

Figure 4.4: Shoot-through duty cycle variation in simulated qZSI model

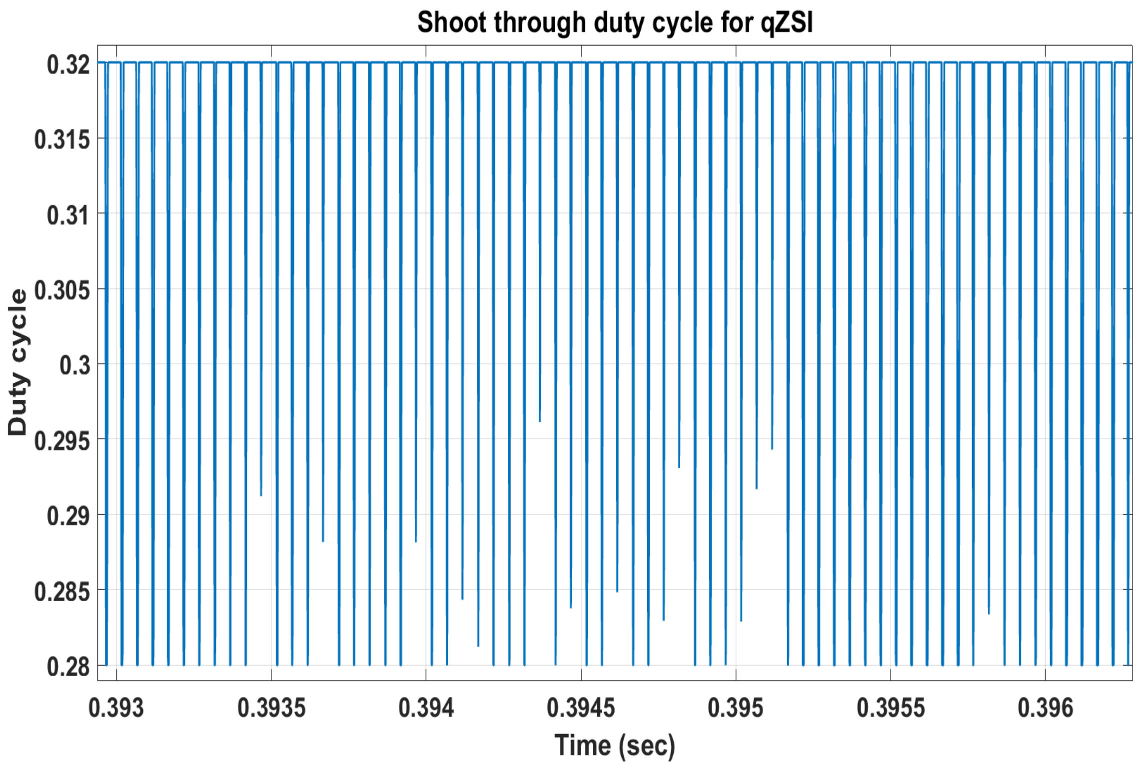

Figure 4.5: Zoomed shoot-through duty cycle variation in simulated qZSI model

It is for most part of the period of 1.2 sec simulation, that the shoot-through duty ratio varies from 0.28 to 0.32 but during the initial part of the Figure 4.4 it is observed to be limited to 0.28. This happens because the input voltage goes to a high value for that duration and hence the boost ratio is less. Consequently the shoot-through has to be limited to the minimum value possible which is 0.28 here. This shoot-through range was obtained by using the boost factor B which is a ratio of the peak DC link voltage to the input voltage of the qZSI i.e. PV array supply voltage to the qZSI. The minimum shoot-through duty ratio also serves as the D_{ini} for the Matlab script(in Appendix B.2.1) used in the controller portion of the qZSI Simulink model.
The Fast Fourier Transform(FFT) was done on the output voltage of the Fronius inverter installed in Chalmers Grundkurs lab. It was observed that apart from the fundamental, the other harmonics that are present include third, fifth and the seventh harmonics which are prominent compared to rest all harmonics. Yet the Total Harmonic Distortion(THD) was even less than 1% for the same inverter. This is in limit as per the standard IEEE STD 519-2014* [35]. The content of the higher harmonics was found nil in the installed inverter output.

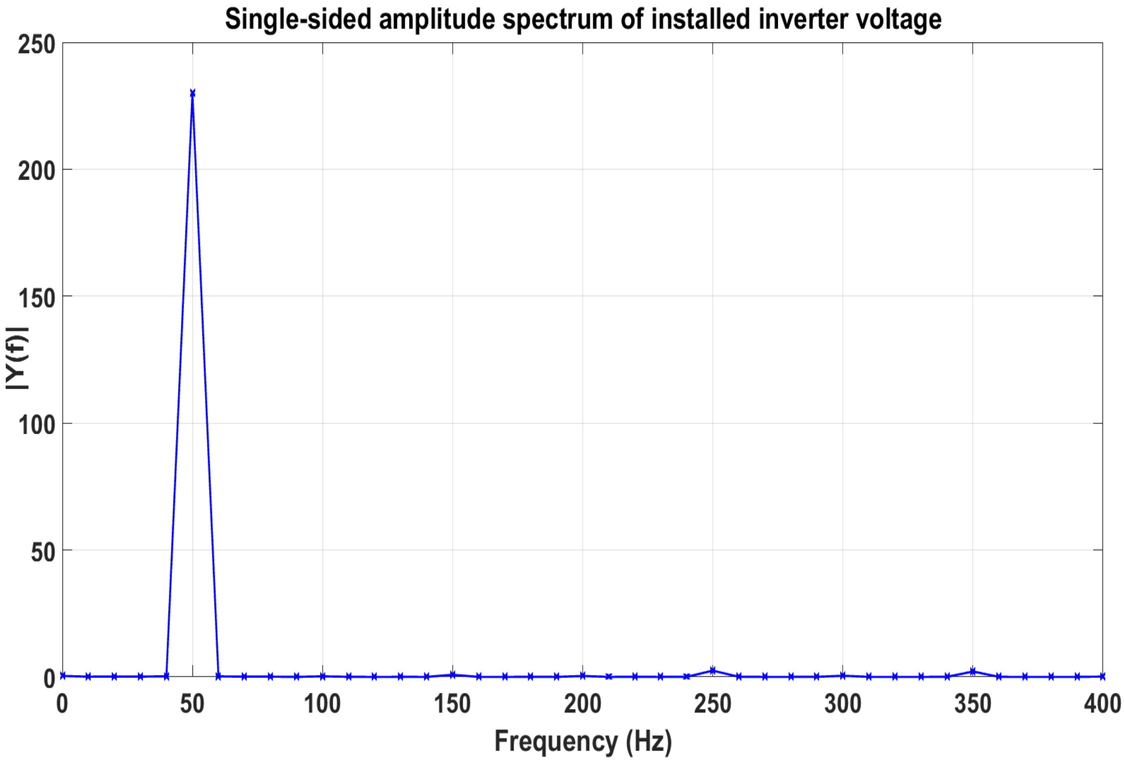

Figure 4.6: FFT of output voltage of the installed inverter in Chalmers lab

The FFT of output voltage of the VSI in reference model* showed minor traces of even and odd harmonics upto the eighth harmonic. The higher harmonics were found absent hence limited to the eighth harmonic in both VSI and qZSI cases. The same can be checked in the Figure 4.7. In comparison the FFT of qZSI output voltage in the simulated model has a more prominent presence of the fifth harmonic with traces of other odd and even harmonics upto the eighth harmonic.

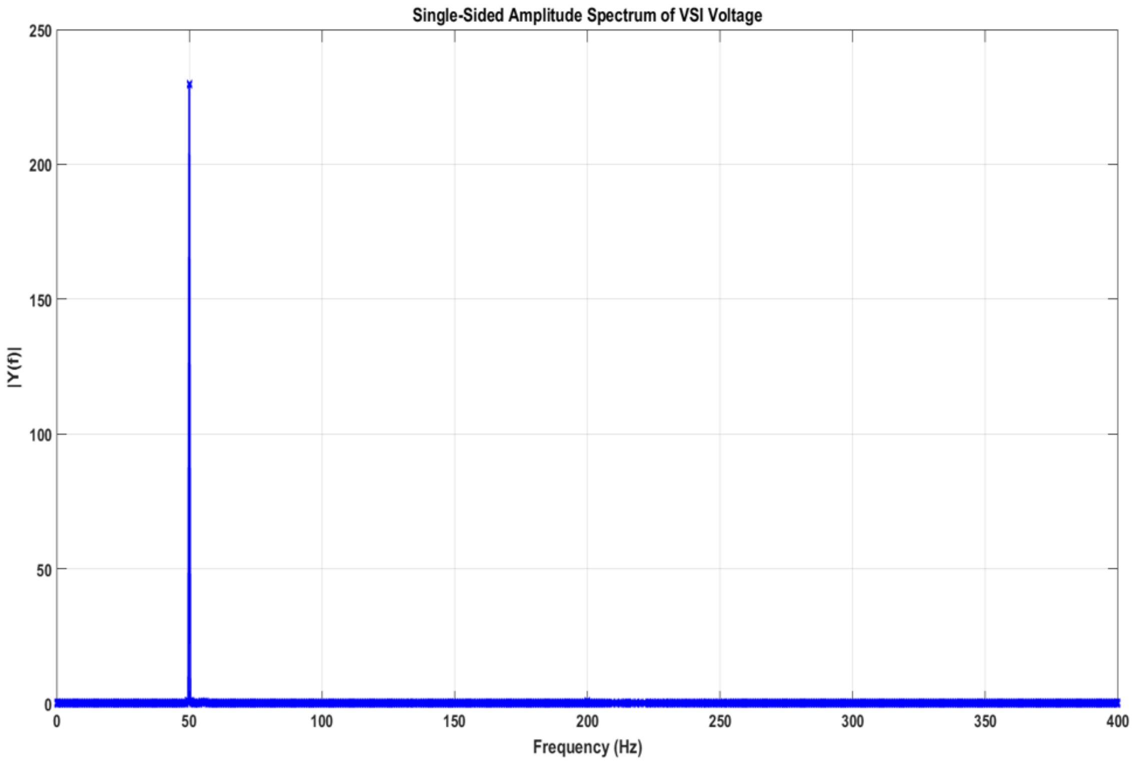

Figure 4.7: FFT of VSI output voltage in reference model*

The prominent presence of the fifth harmonic can be seen in the Figure 4.8 for qZSI.

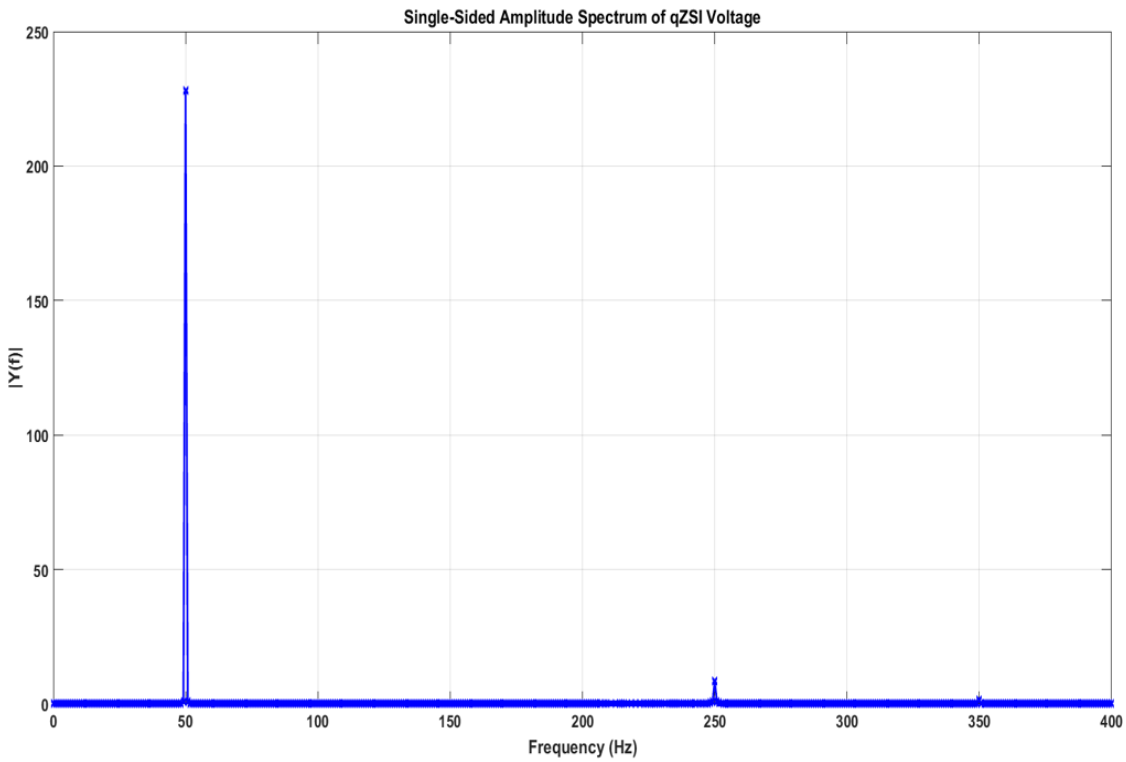

Figure 4.8: FFT of qZSI output voltage in phase 'a

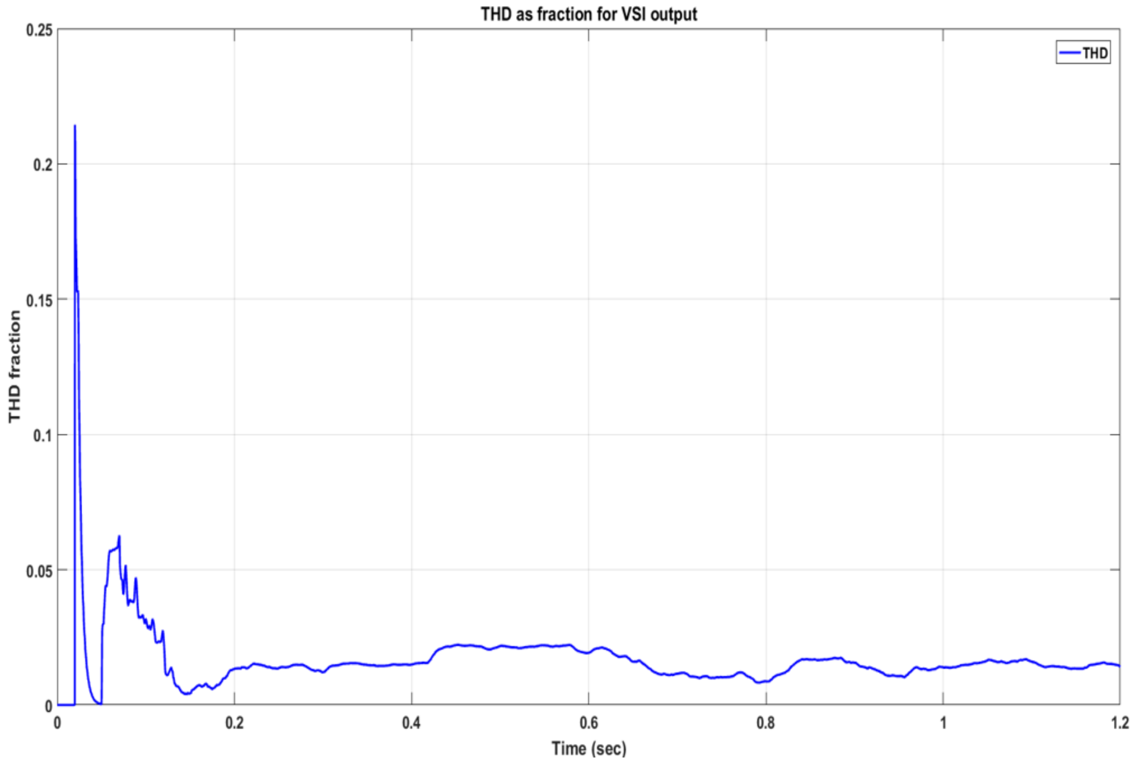

Figure 4.9: THD of VSI output voltage in phase 'a'

The THD value in case of VSI is found to be less than 2.5% under steady state.

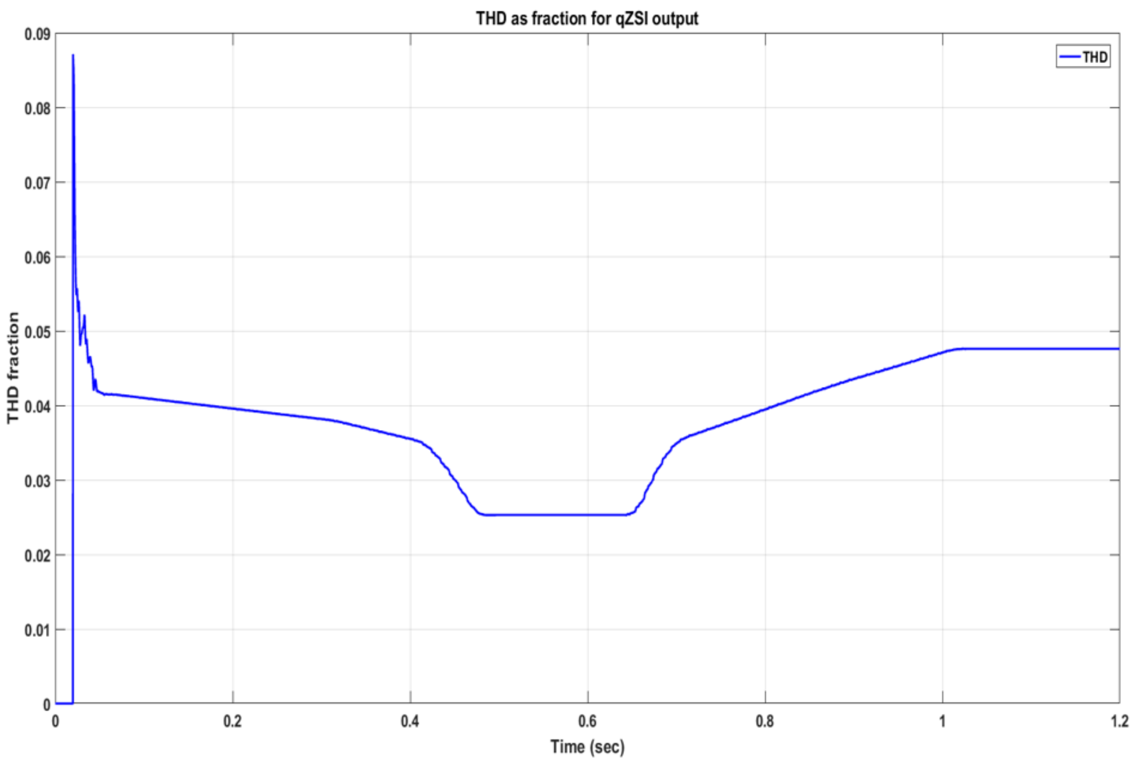

Figure 4.10: THD of qZSI output voltage in phase 'a'

The THD value variation of VSI can be checked in the Figure 4.9.
In Figure 4.8, it can be seen that the presence of fifth harmonic is prominently more than other integer harmonics. The seventh harmonic is also visibly prominent in the same Figure 4.8. It also has higher harmonic distortion compared to the THD of VSI. The THD of qZSI varies between 2.6% to almost 4.8% Figure 4.10. The point to be noted is that the THD of both the models is lower than the prescribed 5% individual harmonic content with the THD % to be less than 8% for voltage $\leq$ 1kV(Here voltage is bus voltage at point of common coupling(PCC)) [35].

Though in case of qZSI, it is observed that harmonic content is more than its counterpart VSI but this can be attributed to a better filtering in the reference model*. More rigorous filtering in qZSI would have although given less THD but the corresponding drop in voltage was also near unavoidable. For the same size of filter, it can be checked if the output of both inverters has the same THD or if the qZSI THD is lower. This will although involve a lot of changes in the VSI reference model* which for example can be ranging from the switching frequency of the boost converter to the VSI switching frequency itself and can be considered one of the future work tasks.

4.2 Sustainable development and ethical aspects

From sustainable point of view, upon comparison if the qZSI output has better efficiency and low harmonic distortion then it is a point of attention. It can lead to certain negative impacts on the environment and society as well.
The solar power production shall increase in the next few years till 2022 as per the International Energy Agency(IEA)[7]. This means that the need for solar cells is going to increase so as to tap more energy. The ill-effects of it on the environment are glaring and the solar energy is not as clean as it might appear. There are three dimensions of sustainable development and they are all affected [9].The economical dimension is affected with an increase in price due to higher demand. This forms a vicious circle where escalated demand and increase in price feed each other. This has negative impact on the people and the environment which are exploited for minting money. Hence strong regulations are needed for its control. The majority of solar cells are produced from quartz which comes from silica. The mining of silica is extremely detrimental to the health of miners causing lung disease like silicosis. Usage of hyrdofluoric acid also causes damage to the tissues of the workers in the factories. It is used to clean the silicon wafers[8]. The new thin film solar cells are not fully environment friendly either. Compounds like cadmium telluride, cadmium sulfide and copper indium gallium selenide(CIGS) are used in their manufacture which have heavy metal cadmium, a carcinogen and genotoxin[8].
It also has ecological dimension where the environment is severely affected. It causes pollution of water supplies due to the formation of silicon tetrachloride, acidifying the soil and production of harmful fumes[8]. The mining also has an ecological dimension. It generally leads to the loss of green cover with low rates of forest cover restoration.
The final dimension is the social dimension[9]. With the increase in demand of min-

erals for the solar cell production and consequent ecological destruction, chances are of brewing a social conflict on the regional and inter-regional level. Thus, a toxic free production of solar cells has to be carried out. The not so sustainable solar cell production is becoming more sustainable slowly with the new technologies to make thin film solar cells. But the impact of increasing qZSI PQ is that demand for both the converter and solar cells will rise. This shall lead to an increase in demand for quartz and feed the circle described in economical dimension before. Thus ecological and economical dimension are connected.

In this work, risks related to ethical aspects were mentioned in the section 1.2.They basically deal with careful data collection, interpretation of the results and ensuring the fair presentation of the Fronius inverter information collected through proper channels.

The output voltage and current data collected during the Fronius IG 15 inverter operation in the Chalmers Grundkurs lab had to be ensured is used for FFT and THD calculation as was collected and no sloppy data management so as to avoid error introduction that would lead to incorrect interpretations. Since data from other sources was also there, it became necessary to avoid any intermixing of it.
The second risk corresponded to possibility of wrong interpretations being drawn from the results data. Hence the it was published and presented separately for all the three inverters compared. The FFT and THD data and plots were generated and showed distinct differences which ensured no mix-ups. The results and plots for qZSI voltage and current on the grid side were again easy to make to figure out distinctlyfor them being the only voltage and current plots from Simulink data. Thus, all analysis happened without any mix-up of results' plots and data.
Finally, majority of the data required for Fronius inverter in order to compare was collected at site and had almost no bearing and impact of the manufacturer which negated chances of influencing it for any gains whatsoever. The parameters were obtained from the manuals, catalogues and purchase order issued by the university. Hence, it can be deemed untainted. The mitigation of this risk ensures more credibility of data and removal of other two risks.

5

Future work and Conclusion

5.1 Future work

The simulation of qZSI model was performed and compared with the reference model* of VSI in Simulink. The design of DC side controller was carried out and the results obtained. But there is always a scope for improvement and future work. Since the model has been made for a DC side controller in qZSI, it can be extended to include AC side controller as well. This will give a chance to counter the disturbances and the faults which might occur in the AC side.
We can also use MPPT voltage with more variations than used in the simulations. Realistic irradiation data from Swedish Meteorological and Hydrological Institute (SMHI) was available at hourly intervals and was hence not used. Data from other sources which is readily available can be used as irradiation source for PV arrays in the model. The sampling frequency can be increased so as to obtain more samples per cycle. The sampling frequency was 10 kHz but can be increased to higher limits which was avoided due to tiime constraints since it took quite some time to collect more samples for higher sampling rate.

The PI controller used in the model has been tuned using the IMC method and was later fine tuned. If fine tuned more, the PI controller can give a better response.
Also the qZSI is an upgraded version of ZSI. It has its advantages compared to the ZSI such as lower value of capacitor C_2 saving costs and continuous DC current but there are other upgrades of ZSI also available which have better performance than the qZSI. Trans-impedance source inverter(TZSI) is another type of ZSI converter that is transformer based. The limitations of qZSI and ZSI are a need for a low modulation index and high boost factor to decrease the voltage stress on the inverter bridge. Presence of an impedance network is also considered a drawback. The answer to such issues is a TZSI which has been derived from the ZSI where the inductors have been replaced by the magnetizing inductances of two transformers whose turns ratio can be used for gain boosting. This TZSI can be further simplified to have only one transformer thus reducing the cost and increasing the voltage boosting ability. Also, in-case of using high switching frequency power devices like SiC transistor and SiC diodes, the power density shall be increased for the TZSIs. Another improvement can be using other strategies like adaptive neuro fuzzy inference(ANFIS) to predict the optimum modulation index and switch angles required for a improved inverter output voltage[36].

5.2 Conclusion

The scope of solar power growth in renewable energy sector is huge considering the sustainable power production being regarded the need of the hour. With danger to the environment and consequently to the humanity, focus has shifted to renewable energy for power production all across the globe. Photovoltaics are the major way to tap the solar energy. Since VSI need a boost converter to step-up the DC voltage prior to conversion, the cascading leads to higher cost. Usage of qZSI and other variants of ZSI is cost effective comparatively.
The design of the impedance network for the qZSI was accomplished by verifying the parameters using pole-zero maps and bode plots. It was further confirmed by value optimization during the simulations.
The PV output varies consequent to the solar irradiation and solar cell temperature. Hence a controller was required to provide a stable DC link voltage for conversion to AC output. Thus, DC side controller was designed for qZSI.
It was designed using the IMC principle and the output AC voltage and current were obtained at a stable level for various variations in input MPPT voltage. Output saturation and anti-windup were considered in the inner current loop design of DC side controller. The lower and upper limit for saturation were derived for the shoot-through duty cycle. Similarly, antiwindup was used to prevent an overshoot in the integrator. Based on their application, stable controller output was achieved.
The MPPT voltage was sampled from the reference model* to supply as input in qZSI model so as to maintain uniformity for fair comparison. Upon FFT of output voltage it was observed that the concentration of lower odd harmonics was more than the inverter installed at the Chalmers Grundkurs lab for both Simulink models.
The inverter installed in the Chalmers lab is a Fronius International GmbH made Fronius IG 15 model. The lab installed inverter had better THD compared to the models, though the limit for THD was not breached under any case by any Simulink model. The reference model* also displayed lesser harmonic distortion compared to qZSI model.

Based on the results obtained, it could be safely ascertained that there is a lot of scope in developing effective control strategies of qZSI and other variants of ZSI for higher efficiency with lower harmonic distortion. The renewable energy is going to see major drive in future.

Bibliography

[1] SMHI, "SMHI Öppna data", Mar 15, 2017. [online]. Available: http://opendata-catalog.smhi.se/explore/

[2] L. Aguilar, "Solar energy in Sweden-an implementation plan", Master's thesis, Institutionen för kulturgeografi och ekonomisk geografi, Lund University, Lund, Sweden, 2013 .

[3] S. Kok, "Examining solar energy policy in China and India: A comparative study of the potential for energy security and sustainable development", Master's thesis, Department of Earth Sciences, Uppsala University, Uppsala, Sweden, 2015.

[4] J. L. Sawin et al, "Renewables 2016 Global status report", REN21, pp. 60-67, 2016.

[5] J. M. Guerrero et al, "Wireless-control strategy for parallel operation of distributed-generation inverters", *IEEE Transaction on Industrial Electronics(IEEE IE)*, pp. 1461–1470, Octo. 2006.

[6] G. Weiss et al, "H^{∞} repetitive control of dc-ac converters in microgrids," *IEEE Transaction on Power Electronics(IEEE TPEL)*, pp. 219-230, Jan. 2004.

[7] International Energy Agency (IEA), "Renewables 2017: Analysis and forecasts to 2022- Executive summary", Market report series, France, Oct. 2017.

[8] D. Mulvaney, "Solar Energy Isn't Always as Green as You Think", IEEE Spectrum, Nov 13, 2014. [online]. Available: https://spectrum.ieee.org/green-tech/solar/solar-energy-isnt-always-as-green-as-you-think

[9] F. Hedenus et al, "Sustainable development: History, definition & the role of the engineer", 2015.

[10] A. Yazdani et al, "Modeling guidelines and a benchmark for power system simulation studies of three-Phase single-stage photovoltaic systems", *IEEE Transaction on Power Delivery(IEEE PWRD)*, Apr. 2011

[11] P. Andersson et al, Inkoppling av solcellsanläggning till elnät, Bachelor's thesis, Institutionen för Energi och Miljö, Chalmers Tekniska Högskola, Göteborg, Sweden, Maj 2007.

[12] E. Twining et al, "Grid current regulation of a three-phase voltage source inverter with an LCL input filter", *IEEE Transaction on Power Electronics(IEEE TPEL)*, pp. 888–895, May 2003.

[13] F. Zheng Peng, "Z-source inverter", IEEE Transaction on Industrial Applications(IEEE IA), pp. 504-510, Mar-Apr. 2003.

[14] P. C. Loh et al, "Transient modeling and analysis of Pulsewidth modulated Z-source inverter", *IEEE Transaction on Power Electronics(IEEE TPEL)*, pp. 498–507, Mar. 2007.

[15] J. Liu et al, "Dynamic modeling and analysis of Z-source converter:Derivation of AC small signal model and design-oriented analysis", *IEEE Transaction on Power Electronics(IEEE TPEL)*, pp. 1786–1796, Sep. 2007.

[16] Y. Li et al, "Modeling and control of Quasi-Z-source inverter for distributed generation applications", *IEEE Transaction on Industrial Electronics(IEEE IE)*, pp. 1532–1541, Apr. 2013.

[17] G. N. V. Prakash, M. K. Kazimierczuk, "Small-signal modeling of open-loop PWM Z-source converter by circuit averaging technique", *IEEE Transaction on Power Electronics(IEEE TPEL)*, pp. 1286–1296, Mar. 2013.

[18] Y. Liu et al, *Impedance Source Power Electronic Converters*, 1st ed., John Wiley & Sons Ltd, 2016, pp. 22-75.

[19] Y. Liu et al, "Z-source/quasi-Z-source inverters:Derived networks, modulations, controls and emerging applications to photovoltaic conversion", *IEEE Industrial Electronics Magazine*, pp. 32–44, Dec. 2014.

[20] S. Bacha, I. Munteanu, A. I. Bratcuet, *Power Electronic Converters Modeling and Control: with Case Studies*, 1st ed., Wiley & Sons Ltd, 2013.

[21] A. Yazdani, R. Iravani, *Voltage-Sourced Converters in Power Systems: Modeling, Control and Applications*, 1st ed., Wiley & Sons Ltd, 2010.

[22] M. Mosa et al, "High performance predictive control applied to three phase grid connected Quasi-Z-source inverter", *In Annual Conference of the IEEE Industrial Electronics Society(IEEE IECON 2013)*, pp. 5812–5817, 2013.

[23] Y. Li et al, "Modeling and control of Quasi-Z-source inverter for distributed generation applications", *IEEE Transaction on Industrial Electronics(IEEE*

IE), pp. 1532–1541, Apr. 2013.

[24] X. Ding et al, “A direct dc-link boost voltage PID-like fuzzy control strategy in Z-source inverter”, *In IEEE on Power Electronics Specialists Conference(IEEE PESC 2008)*, pp. 405–411, 2008.

[25] C. J. Gajanayake et al, “Development of a comprehensive model and a multiloop controller for Z-source inverter DG systems”, *IEEE Transaction on Industrial Electronics(IEEE IE)*, pp. 2352–2359, Aug 2007.

[26] Q. V. Tran et al, “Minimization of voltage stress across switching devices in the Z-source inverter by capacitor voltage control”, *Journal of Power Electronics(JPE)*, pp. 335–342, May 2009.

[27] H. Abu-Rub et al, “Quasi-Z-source inverter-based photovoltaic generation system with maximum power tracking control using ANFIS”, *IEEE Transaction on Sustainable Energy(IEEE STE)*, pp. 11–20, Jan.2 013.

[28] H. Rostami et al, “Neural networks controlling for both the DC boost and AC output voltage of Z-source inverter”, *In of the Power Electronics Drive Systems and Technologies Conference(PEDSTSC 2010)*, pp. 135–140, Feb. 2010.

[29] A. H. Rajaei et al, “Sliding-mode control of Z-source inverter”, *In of IEEE Annual Conference on Industrial Electronics(IEEE IECON 2008)*, pp. 947–952, Nov. 2008.

[30] J. Liu et al, “A digital current control of Quasi-Z-source inverter with battery”, *IEEE Transaction on Industrial Informatics(IEEE II)*, pp. 928–937, May 2013.

[31] F. Z. Peng et al, “Maximum boost control of the Z-source inverter”, *IEEE Transaction on Power Electronics(IEEE TPEL)*, pp. 833–838, Jul-Aug. 2005.

[32] M. S. Shen et al, “Constant boost control of the Z-source inverter to minimize current ripple & voltage stress”, *IEEE Transaction on Industrial Applications(IEEE IA)*, pp. 770-778, May-Jun. 2006.

[33] S.L. Sanjuan, “Voltage Oriented Control of Three-Phase Boost PWM Converters”, Master’s thesis, Department of Energy and Environment, Chalmers University of Technology, Gothenburg, Sweden, 2010.

[34] Y. Liu et al, “Modeling and SVPWM control of Quasi-Z-source inverter”, *In International Conference on Electrical Power Quality and Utilisation(EPQU 2011)*, pp. 1–7, 2011.

[35] "IEEE Std 519-2014(Revision of IEEE Std 519-1992)-IEEE recommended practice and requirements for harmonic control in electric power systems", Mar. 15, 2014. [online]. Available: https://standards.ieee.org/findstds/standard/519-2014.html

[36] T.R.Sumithira, A.N. Kumar "Elimination of harmonics in multilevel inverters connected to solar photovoltaic systems using ANFIS: An experimental case study", *Journal of Applied Research & Technology*, pp. 124-132, Feb. 2013.

[37] S. B. Kjaer, "Design and Control of an Inverter for Photovoltaic Applications", PhD thesis, Institut for Energiteknik, Aalborg Universitet, Aalborg, Denmark, 2005.

[38] M. A. Hussain et al. "Comparative assessment of maximum power point tracking procedures for photovoltaic systems", *Green Energy & Environment*, pp. 5-17, Jan. 2017.

A

Appendix

A.1 IEEE Standard STD 519-2014

For the voltage V at point of common coupling(PCC) the individual harmonic content should be less than 5% and the THD should be less than 8% such that V$\leq$ 1kV[35].

A.2 Maximum power point tracking(MPPT)

In distributed power generation like PV array, power generated is susceptible to variation in the irradiance(W/m^2) and temperature of the PV cells.

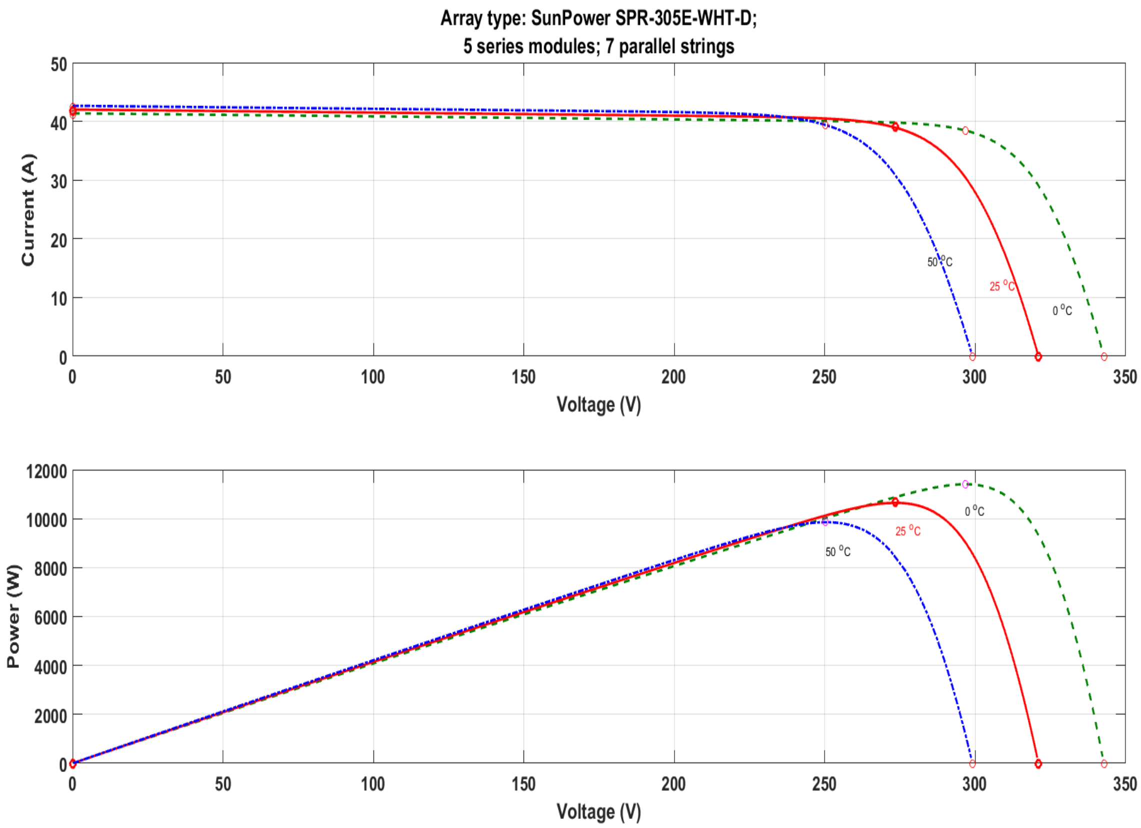

Figure A.1: I-V and P-V characteristic plot of PV array used in simulation.

The maximum power extraction through PV array is hence a method of varying the resistance visible(of the connected load) to the PV array so that the operating point and the maximum power point coincide or are closeby for the respective array.
The PV array used in the reference model* is **SunPower SPR-305E-WHT-D** with I-V and P-V characteristics as shown in Figure A.1.
In order to extract maximum power from the PV array a multitude of MPPT models are used. Of all the MPPT models, most common are the following four models:

- Perturb and observe/Hill climbing
- Incremental conductance
- Current Sweep and
- Constant voltage.

The MPPT algorithm is applied for DC-DC boost converter followed by a VSI controlling the duty cycle of the boost converter in the reference model*. For the qZSI, sampled MPPT voltage from the reference model* is used as input.In the MPPT logic variation of duty cycle is employed to vary the observed resistance(reflected on the PV array side). The variation in duty cycle and hence resistance leads to coincidence of the actual load line with the load line passing through the maximum power point. Since incremental conductance logic is used in simulations, only it has been explained below. There are other models as well like Droop method, Fuzzy logic based, Neural network based, Particle swarm optimization MPPT, et cetra. The other MPPT logics can be accessed at [37] and [38].

A.2.1 Incremental conductance

During the modelling of MPPT controller, incremental conductance logic is utilized. The current can be expressed as a function of voltage $i_{PV} = F(u_{PV})$. At the maxima of the P-V characteristic plot, the gradient or the first order differential of Power P to voltage u_{PV} is equal to zero. The same property is utilized to arrive at the conclusion that at the maximum power point, the instantaneous conductance value $(-i_{PV}/u_{PV})$ and the incremental conductance value (di_{PV}/du_{PV}) are the same. This is shown in the eqn A.1.

$$\begin{aligned}
\frac{dP_{PV}}{du_{PV}} &= 0 \\
\frac{(du_{PV}).(di_{PV})}{du_{PV}} &= 0 \\
i_{PV} + \frac{di_{PV}}{du_{PV}}.u_{PV} &= 0 \\
\frac{di_{PV}}{du_{PV}} &= -\frac{i_{PV}}{u_{PV}} \\
\frac{\Delta i_{PV}}{\Delta u_{PV}} &= -\frac{i_{PV}}{u_{PV}}
\end{aligned} \tag{A.1}$$

A.3 Matlab Script

A.3.1 Duty cycle function in controller subsystem

```
function y = fcn(u)

persistent Dini;

if isempty(Dini)
Dini = 0.28;
u = Dini;
y = Dini;
else
Dini = u;
y = Dini;
end
```